

Primordial Black Holes from a tiny bump/dip in the Inflaton potential

Swagat S. Mishra^a and Varun Sahni^a

^aInter-University Centre for Astronomy and Astrophysics, Post Bag 4, Ganeshkhind, Pune 411 007, India

E-mail: swagat@iucaa.in, varun@iucaa.in

Abstract. Scalar perturbations during inflation can be substantially amplified by tiny features in the inflaton potential. A bump-like feature behaves like a local speed-breaker and lowers the speed of the scalar field, thereby locally enhancing the scalar power spectrum. A bump-like feature emerges naturally if the base inflaton potential $V_b(\phi)$ contains a local correction term such as $V_b(\phi) [1 + \varepsilon(\phi)]$ at $\phi = \phi_0$. The presence of such a localised correction term at ϕ_0 leads to a large peak in the curvature power spectrum and to an enhanced probability of black hole formation. Remarkably this does not significantly affect the scalar spectral index n_s and tensor to scalar ratio r on CMB scales. Consequently such models can produce higher mass primordial black holes ($M_{\text{PBH}} \geq 1M_\odot$) in contrast to models with ‘near inflection-point potentials’ in which generating higher mass black holes severely affects n_s and r . With a suitable choice of the base potential – such as the string theory based (KKLT) inflation or the α -attractor models – the amplification of primordial scalar power spectrum can be as large as 10^7 which leads to a significant contribution of primordial black holes (PBHs) to the dark matter density today, $f_{\text{PBH}} = \Omega_{0,\text{PBH}}/\Omega_{0,\text{DM}} \sim O(1)$. Interestingly, our results remain valid if the bump is replaced by a dip. In this case the base inflaton potential $V_b(\phi)$ contains a negative local correction term such as $V_b(\phi) [1 - \varepsilon(\phi)]$ at $\phi = \phi_0$ which leads to an enhanced probability of PBH formation. We conclude that primordial black holes in the mass range $10^{-17}M_\odot \leq M_{\text{PBH}} \leq 100 M_\odot$ can easily form in single field inflation in the presence of small bump-like and dip-like features in the inflaton potential.

Keywords: Inflation, Primordial black holes, Dark matter, Early universe

Contents

1	Introduction	1
2	Primordial Black Hole formation in single field Inflation	3
2.1	Inflationary model building for generating primordial black holes	3
3	PBHs from a bump/dip in the inflaton potential	8
3.1	Primordial black holes from KKL _T Inflation	9
3.2	Primordial black holes from α -attractor Inflation	12
3.3	Primordial black holes from a dip in the inflaton potential	14
3.4	Formation and abundance of primordial black holes	16
4	Discussion	23
A	The Mukhanov-Sasaki Equation	25
B	Primordial black hole formation and abundance	26

1 Introduction

The existence of primordial black holes (PBHs) has been a subject of considerable interest ever since this possibility was suggested by Zeldovich and Novikov in 1967 [1]. Subsequently Hawking [2] showed that quantum evaporation would leave behind PBHs with masses greater than about 10^{15} g, smaller black holes having completely evaporated by the present epoch. Interest in PBHs grew quite rapidly following these two seminal papers [3–11]. It was soon realized that PBHs created in the early history of our universe could be of considerable importance since they might:

1. Seed the formation of supermassive black holes (BHs) in the nuclei of galaxies and AGN’s [12, 13].
2. Influence the ionization history of the universe [14, 15].
3. Contribute to the dark matter (DM) density in the universe [16, 17].

One might add that since particle dark matter in the form of WIMPs or an axion has not yet been compellingly discovered either by accelerator experiments or by direct DM searches, the possibility that a significant component of DM may consist of primordial black holes presents an entirely plausible and even alluring possibility [18–33].

Interest in PBHs received a major boost with the discovery by LIGO of gravitational radiation from merging BHs (event GW150914) with a mass of about $30M_{\odot}$ [34]. This discovery was supported by additional events and, at the time of writing, the number of black hole merger events exceeds ten, with many more expected to follow from future runs of LIGO, Virgo and KAGRA. For constraints on PBH abundance using stochastic gravitational wave background (SGWB) from binary PBH mergers, see [35, 36].

The precise physical mechanism responsible for PBH formation has also been a subject of considerable debate and reference to early work can be found in the reviews [37, 38].

Early models of PBH production included: formation during bubble collision in a first order phase transition, the collapse of topological defects such as domain walls and cosmic strings, etc. Within the context of inflation, it was suggested that an enhancement of perturbations leading to PBH formation would occur if the inflationary spectrum had a significant blue tilt and/or non-Gaussianity, or if the inflaton rolled extra slowly for a duration of time which was much shorter than the full inflationary epoch [39–43]. This last possibility can be realized in several ways some of which have been discussed in models of ‘designer inflation’ [39–43].

In the context of single-field models, PBHs can form if the potential contains a near inflection point, or a saddle type region, which slows the motion of the inflaton field and leads to a spike in the perturbation spectrum [44–50].

Alternatively, the inflaton can also slow down by climbing a small local bump-like feature in the base inflationary potential. As we show in this paper, by locally slowing the motion of the scalar field, the bump behaves like a speed-breaker and leads to a sharp increase in the amplitude of the curvature perturbation \mathcal{R} . An interesting example of a local speed-breaker arises if a term such as $V_b(\phi)\varepsilon(\phi)$ ($\varepsilon \ll 1$), localised at $\phi = \phi_0$, is added to the base inflationary potential $V_b(\phi)$. Applying this simple prescription to the string theory¹ based KKLT model [52, 53] and to α -attractor potentials [54, 55] we find a sharp local enhancement of primordial perturbations at ϕ_0 which can result in a significant abundance of PBHs at the present epoch. The local nature of the speed-breaker permits the generation of PBHs in a wide mass range ranging from the ultra-light $10^{-17} M_\odot$ to the super-heavy $10^2 M_\odot$ without significantly affecting n_s and r on CMB scales. This stands in marked contrast to ‘near inflection point’ scenarios which have difficulty in producing large mass PBHs without introducing a significant red tilt into the primordial perturbation spectrum on CMB scales.²

Interestingly, a tiny local dip-like feature, which originates when a term such as $V_b(\phi)\varepsilon(\phi)$ ($\varepsilon \ll 1$), localised at $\phi = \phi_0$, is subtracted from the base inflationary potential $V_b(\phi)$, also serves the purpose of PBH formation. In this case the inflaton slows down while surmounting the dip, resulting in the amplification of the scalar power spectrum and the production of PBHs. Thus both bumps and dips in the inflaton potential can successfully generate PBHs in a variety of mass-ranges.

Our paper is organised as follows. Section 2 discusses the methodology of PBH formation in single field inflation. Section 3 applies this methodology to our model, based on speed-breaker potentials. Our results are summarized in section 4. The two appendices elaborate on the use of the Mukhanov-Sasaki formalism as well as the Press-Schechter approach both of which have been used in this paper to determine the PBH mass function.

We assume the background universe to be spatially flat, homogeneous and isotropic with the metric signature $(-, +, +, +)$ and work in the units $c, \hbar = 1$ and $m_p = \frac{1}{\sqrt{8\pi G}}$.

¹See [51] for PBH formation in the framework of String Theory, based on near inflection point potential.

²In order to make our terminology more transparent, it is important to note that a pure inflection point potential under-produces PBHs. In order to generate cosmologically abundant PBHs in this scenario one also requires the inflaton to climb a local maximum in the potential [49]. However this PBH feature is intrinsically inbuilt into the full potential and it is very nearly impossible to separate the feature from the base potential. We refer to such models as ‘near inflection point’ models. By contrast, in our model (3.1), the PBH feature is essentially local and the full potential can always be thought of as a base inflationary potential with a tiny local bump/speed-breaker superimposed on it.

2 Primordial Black Hole formation in single field Inflation

PBHs are formed when sufficiently large primordial density fluctuations (usually quantified in terms of the comoving curvature perturbation \mathcal{R}) enter the Hubble radius during the radiation dominated epoch. PBH formation within the context of inflation usually involves two important steps:

1. Generation of large primordial scalar fluctuations \mathcal{R} on a length scale $k_{\text{PBH}} \gg k_*$ during inflation, where k_* is the CMB pivot scale.
2. The post-inflationary collapse of Hubble-size overdense regions (and formation of PBHs) after the horizon re-entry of the fluctuation mode k_{PBH} .

In this section we map out the basic methodology and relevant formulae concerning step 1. In section 3 we introduce our model potentials and apply step 2 to them in section 3.4 in order to compute PBH mass function.

2.1 Inflationary model building for generating primordial black holes

In the standard single field inflationary paradigm, inflation is sourced by a minimally coupled canonical scalar field ϕ with a suitable potential $V(\phi)$. The background evolution of the scalar field and the scale factor of the universe is given by the following set of cosmological equations

$$H^2 = \frac{1}{3m_p^2}\rho_\phi = \frac{1}{3m_p^2} \left[\frac{1}{2}\dot{\phi}^2 + V(\phi) \right], \quad (2.1)$$

$$\dot{H} = \frac{\ddot{a}}{a} - H^2 = -\frac{1}{2m_p^2}\dot{\phi}^2, \quad (2.2)$$

$$\ddot{\phi} + 3H\dot{\phi} + V'(\phi) = 0. \quad (2.3)$$

The extent of inflation is indicated by the total number of e-foldings during inflation

$$\Delta N_e = N_e^i - N_e^{\text{end}} = \log_e \frac{a_{\text{end}}}{a_i} = \int_{t_i}^{t_{\text{end}}} H(t) dt, \quad (2.4)$$

where $H(t)$ is the Hubble parameter during inflation. N_e denotes the number of e-foldings before the end of inflation so that $N_e = N_e^i$ corresponds to the beginning of inflation while $N_e = N_e^{\text{end}} = 0$ corresponds to the end of inflation. a_i and a_{end} denote the scale factor at the beginning and end of inflation respectively. Typically a period of quasi-de Sitter inflation lasting for at least 60-70 e-foldings is required in order to address the problems of the standard hot Big Bang model. We denote N_* as the number of e-foldings (before the end of inflation) when the CMB pivot scale $k_* = (aH)_* = 0.05 \text{ Mpc}^{-1}$ left the comoving Hubble radius during inflation. For convenience we have chosen $N_* = 60$. The quasi-de Sitter like phase corresponds to the inflaton field rolling slowly down the potential $V(\phi)$ ³. This slow-roll phase of inflation, ensured by the presence of the Hubble friction term in the equation (2.3), is usually characterised by the first two Hubble slow-roll parameters ϵ_H, η_H

³It is well known that the slow-roll phase of the inflation is actually a local attractor for many different models of inflation, see [56] and references therein.

[57]

$$\epsilon_H = -\frac{\dot{H}}{H^2} = \frac{1}{2m_p^2} \frac{\dot{\phi}^2}{H^2}, \quad (2.5)$$

$$\eta_H = -\frac{\ddot{\phi}}{H\dot{\phi}} = \epsilon_H + \frac{1}{2\epsilon_H} \frac{d\epsilon_H}{dN_e}, \quad (2.6)$$

where

$$\epsilon_H, \eta_H \ll 1, \quad (2.7)$$

during the slow-roll regime. During slow-roll scalar field perturbations are usually quantified in terms of the comoving curvature perturbation \mathcal{R} and its power spectrum [57]

$$P_{\mathcal{R}} = \frac{1}{8\pi^2} \left(\frac{H}{m_p} \right)^2 \frac{1}{\epsilon_H}. \quad (2.8)$$

A more accurate determination of $P_{\mathcal{R}}$ is provided by solving the Mukhanov-Sasaki equation given by [58, 59]

$$v_k'' + \left(k^2 - \frac{z''}{z} \right) v_k = 0 \quad (2.9)$$

where

$$v \equiv z\mathcal{R}, \quad \text{with} \quad z = a \frac{\dot{\phi}}{H}, \quad (2.10)$$

and

$$P_{\mathcal{R}} = \frac{k^3}{2\pi^2} \frac{|v_k|^2}{z^2} \Big|_{k \ll aH}, \quad (2.11)$$

see appendix A for details.

On the large cosmological scales which are accessible to CMB observations, the power spectrum typically takes the form of a power law represented by

$$P_{\mathcal{R}}(k) = A_S \left(\frac{k}{k_*} \right)^{n_S - 1}, \quad (2.12)$$

where $A_S = P_{\mathcal{R}}(k_*)$ is the amplitude of the scalar power spectrum at the pivot scale. The scalar spectral tilt n_S and the tensor to scalar ratio r , in the slow-roll regime, are given by [57]

$$n_S = 1 + 2\eta_H - 4\epsilon_H, \quad (2.13)$$

$$r = 16 \epsilon_H. \quad (2.14)$$

Recent CMB observations [60, 61] suggest $A_S = 2.1 \times 10^{-9}$, $n_S \simeq 0.965$ and $r < 0.1$ at the CMB pivot scale k_* . The relatively low upper bound on the tensor to scalar ratio tends to favor potentials which are concave and asymptotically flat, an example being shown in the left panel of figure 1. Such simple slow-roll potentials satisfy CMB constraints on large scales around $\phi = \phi_*$ and do not possess any peculiar features on smaller scales until inflation ends at $\phi = \phi_{\text{end}}$. The slow-roll condition (2.7) remains valid for most part of the potential and is violated only towards the end of inflation as shown in the left panel of figure 2. These models

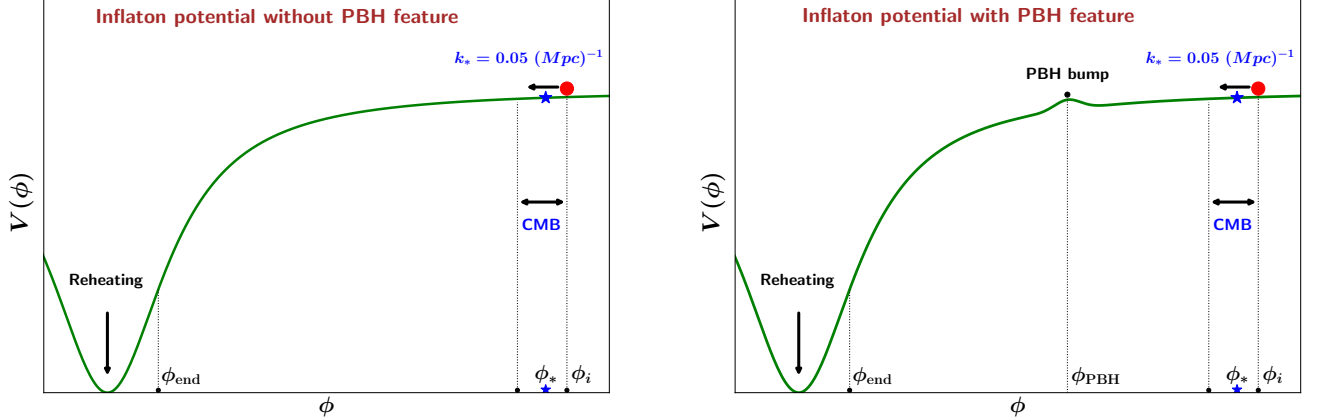


Figure 1: **Left panel:** illustrates a portion of the KKLt inflationary potential (3.2). The potential is concave and asymptotically flat and does not possess any intermediate scale feature between ϕ_* and ϕ_{end} . The portion of the potential accessible to CMB observations is shown by dotted vertical lines around the pivot scale value of the field ϕ_* (indicated by a blue color star). **Right panel:** shows the same potential with a PBH feature in the form of a local bump (3.3) superimposed on it. The feature arises at an intermediate scalar field value ϕ_{PBH} before the end of inflation ϕ_{end} . Note that the bump size is shown significantly amplified for the purposes of illustration.

predict a smooth scalar power-spectrum $P_{\mathcal{R}}$ which monotonically decreases from the largest scales ($N_e \sim N_*$) to the smallest scales ($N_e \simeq 0$) as shown in the right panel of figure 2.

During slow roll inflation, the comoving Hubble radius $(aH)^{-1}$ falls as the universe expands quasi-exponentially. This leads to the Hubble radius exit of primordial fluctuations with comoving wave number k (see figure 3). After inflation ends, the universe begins to decelerate and the comoving Hubble radius grows with time. As a result fluctuation modes which had exited the Hubble radius during inflation re-enter it during deceleration, leading eventually to the formation of galaxies and the cosmic web. It is instructive that CMB observations probe only about 7-8 e-folds of inflation, corresponding to a small section $\Delta\phi$ around the pivot scale value ϕ_* of the potential, as shown in the left panel of figure 1. The remaining 50 e-folds of expansion until the end of inflation remain virtually inaccessible to CMB observations.

PBHs can form due to a feature in the inflationary potential on these smaller scales. For instance, a feature in the inflationary potential in the form of a local bump (which is the primary focus of this work) shown in the right panel of figure 1, can slow down the already slowly rolling inflaton field substantially. A large drop in the value of $\dot{\phi}$ (with little change in the value of H) during inflation, causes ϵ_H to drop appreciably from its pivot scale value and leads to a substantial enhancement of the scalar power $P_{\mathcal{R}}$ as suggested by equation (2.8).

The following criteria need to be satisfied so that an inflationary potential can generate fluctuations which are large enough to seed PBH formation [38, 47, 49, 50].

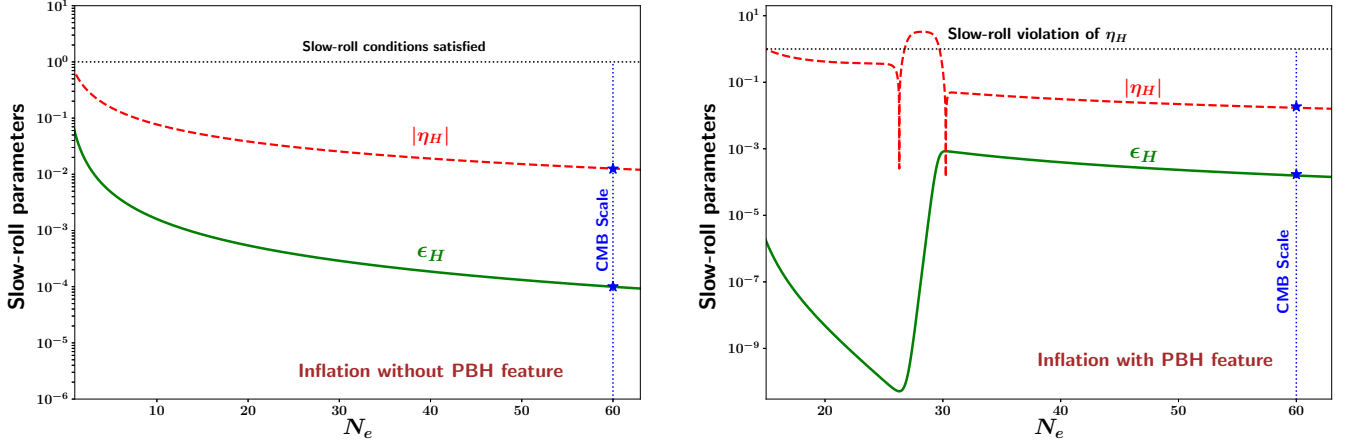


Figure 2: **Left panel:** shows that the slow-roll conditions (2.7) remain satisfied during KKLT inflation (3.2) whose potential is shown in the left panel of figure 1. **Right panel:** demonstrates the violation of the slow-roll conditions (2.7) during the formation of $10^{-13} M_\odot$ PBHs due to the presence of a feature in the form of a Gaussian bump (characterised by parameters in the second row of table 1) in the KKLT potential (3.4); see the right panel of figure 1. Note that while ϵ_H (solid green) always remains $\ll 1$, $|\eta_H|$ (red dashed) becomes greater than $O(1)$ during power amplification due to the sharp drop in the value of ϵ_H near the bump. This leads to the breakdown of the slow-roll approximation, as originally shown in a different context in [48].

- Compatibility with large scale CMB observations [60, 61] requires the potential to satisfy the conditions

$$n_s \in (0.956, 0.978) \quad , \quad r(k_*) \leq 0.06 \quad \text{at } 95\% \text{ C.L} \quad (2.15)$$

and

$$P_{\mathcal{R}}(k_*) = 2.1 \times 10^{-9} \quad (2.16)$$

where $k_* = (aH)_* = 0.05 \text{ Mpc}^{-1}$ marks the pivot scale.

- A feature in $V(\phi)$ is required on a smaller scale $k \gg k_*$ ($N_e < N_*$) to enhance the primordial scalar power spectrum by a factor of about 10^7 with respect to its value at the CMB pivot scale. This feature could be in the form of a near inflection point, an intermediate plateau, or a local bump. The latter is discussed in detail later in this work and is illustrated in the right panels of figures 1 and 4.
- A minimum in the potential marking the end of inflation and a transition (via reheating) to radiation dominated expansion.

PBH formation requires the enhancement of the inflationary power spectrum by a factor of 10^7 within less than 40 e-folds of expansion (on scales smaller than the pivot scale N_*). Therefore the quantity $\Delta \ln \epsilon_H / \Delta N$, and hence also $|\eta_H|$, can grow to become of order unity

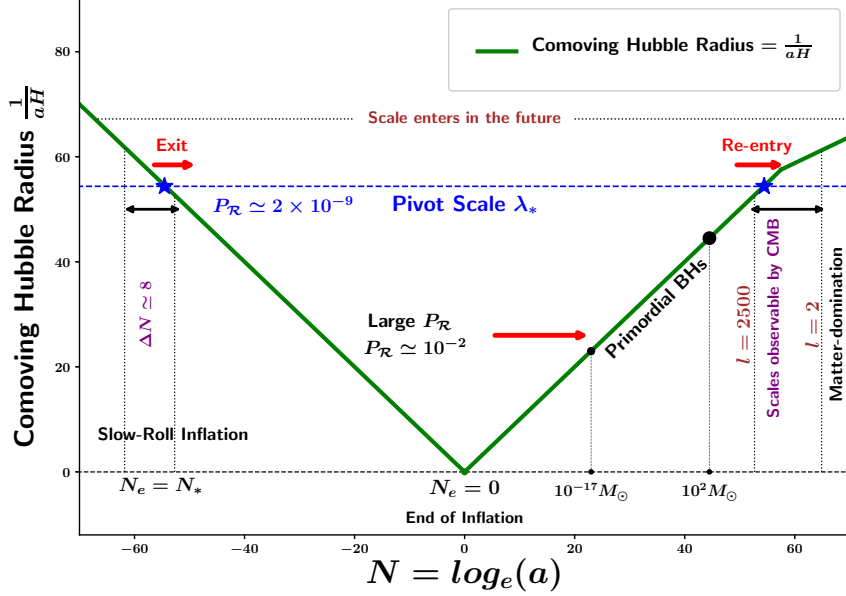


Figure 3: The comoving Hubble radius is plotted as a function of scale factor starting from quasi-de Sitter inflation until the matter dominated epoch (assuming instant reheating at the end of inflation). The figure illustrates different comoving wavelengths leaving the Hubble radius during inflation and re-entering later during the radiation and matter dominated epochs. The pivot scale is shown by the blue color dotted line and stars. This figure illustrates the fact that only a small fraction of the inflationary epoch, $\Delta N \simeq 7 - 8$, (shown within vertical dotted lines around the pivot scale) is accessible to CMB observations. PBHs form on much smaller scales.

thereby violating the slow-roll condition (2.7), as originally shown in [48]. In fact the second Hubble slow-roll parameter $|\eta_H|$ becomes larger than unity even though ϵ_H itself remains much smaller than unity (see the left panel of figure 4). As a result, equation (2.8) can no longer be trusted to compute the power spectrum and one must determine $P_{\mathcal{R}}$ by numerically integrating the Mukhanov-Sasaki equation (2.9); see appendix A for details. Figures 2 and 4 illustrate this result for two models: (i) standard slow-roll inflation fuelled by the KKLT potential (3.2) (see left panel of figure 1), (ii) a tiny bump (3.3) on top of the KKLT potential (see the right panel of figure 1). From the right panels of 2 & 4 one sees that the slow-roll formula (2.8) underestimates the amplitude of power enhancement as well as the location of the peak in $P_{\mathcal{R}}$. This, in turn, leads to a miscalculation of the mass M_{PBH} and abundance f_{PBH} of primordial black holes, as demonstrated in section 3.4.

Once seed fluctuations for PBH formation (in terms of an enormously amplified $P_{\mathcal{R}}$) are successfully generated during inflation, the next step is to determine the abundance of PBHs formed upon the horizon re-entry of seed fluctuation modes. This is done by using the Press-Schechter formalism discussed in section 3.4.

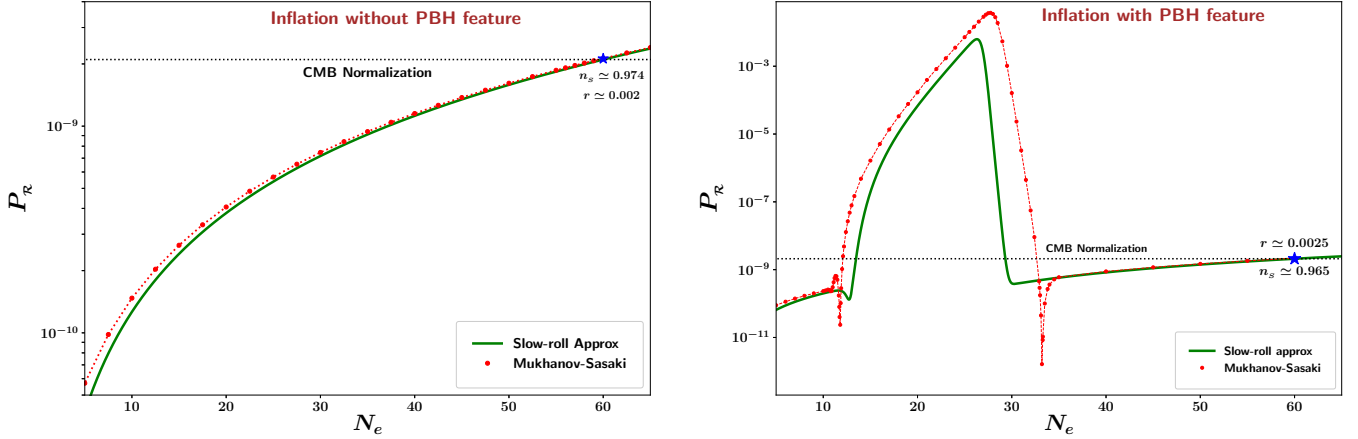


Figure 4: **Left panel:** the scalar power spectrum $P_{\mathcal{R}}$ is determined: (a) by using the slow-roll approximation (2.8) (solid green) and (b) by numerically solving the Mukhanov-Sasaki equation (2.9) & (2.11) (red dots) for the base KKLT inflation potential (3.2). $P_{\mathcal{R}}$ is plotted as a function of the number of e-folds before the end of inflation N_e . Note that both methods give identical results for a smoothly varying potential, in which case $P_{\mathcal{R}}$ decreases monotonically with decreasing N_e . **Right panel:** shows the plot of the scalar power spectrum during the formation of $10^{-13} M_{\odot}$ PBHs in our model (3.4). This panel demonstrates that the slow-roll formula (2.8), shown in solid green, miscalculates the amplitude as well as the peak position of $P_{\mathcal{R}}$. Therefore one must numerically solve the Mukhanov-Sasaki equation (dotted red) in order to compute $P_{\mathcal{R}}$ accurately (see appendix A).

3 PBHs from a bump/dip in the inflaton potential

Our model for PBH formation from a tiny local bump is based on a potential having the general form⁴

$$V(\phi) = V_b(\phi) [1 + \varepsilon(\phi)] \quad (3.1)$$

where V_b is the base inflationary potential responsible for generating quantum fluctuations compatible with the CMB constraints on n_s , r . The term $\varepsilon(\phi) \ll 1$ describes a tiny bump in the potential at ϕ_0 having width σ , see (3.3).

For simplicity we shall work with an asymptotically flat concave base potential which is locally modified by a Gaussian bump⁵. Note that the base potential should satisfy $0.956 \leq n_s \leq 0.978$. This permits the successful generation of small scale fluctuations while ensuring that the CMB 2σ bound on n_s is not violated. It is interesting that a base potential with a flatter tilt of $n_s \geq 0.98$, which is in tension with CMB observations, **becomes strongly favored** when it is modified with a bump. This arises because the amplification of power near the bump typically generates 10-15 extra e-foldings which pulls the CMB pivot scale ϕ_*

⁴We have considered this general form of the potential as a phenomenological model. However it might be possible to find a physical mechanism where the bump-like feature is a small local radiative correction to the base potential.

⁵One can also model the bump using other functional forms such as $\varepsilon \sim 1/\cosh^2[(\phi - \phi_0)/\sigma]$, etc.

closer to ϕ_{end} and leads to a decrease in the value of n_s , as shown in figure 6. We commence our discussion with string theory based KKLT inflation [52, 53, 62–65] as our base potential, even though other potentials, like the α -attractors [54, 55] are also suitable for our purpose and will be discussed later in the text. Note that the n_s and r values will be different for different base potentials, and a base potential with a large red tilt $n_s < 0.96$ will not be suitable for generating PBHs in our model.

3.1 Primordial black holes from KKLT Inflation

In our first example, the base potential in (3.1) is associated with KKLT inflation [65]

$$V_b(\phi) = V_0 \frac{\phi^n}{\phi^n + M^n}, \quad (3.2)$$

where V_0 fixes the overall CMB normalization given by equations (2.8) & (2.16). The n_s and r values of the base potential are shown in red color in figure 5 for $n = 2$. Although the base potential (3.2) has two free parameters M and n , we shall set $M = m_p/2$ and $n = 2$, for simplicity. The potential (3.2) with the pivot scale value ϕ_* is shown by the black color dashed curve in the left panel of figure 6.

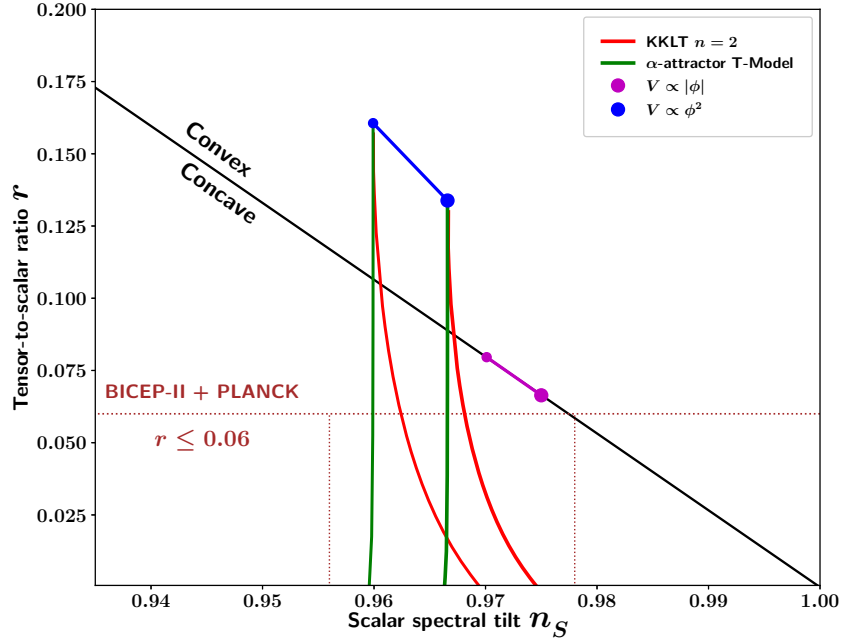


Figure 5: CMB pivot scale values of the tensor to scalar ratio r and scalar spectral tilt n_s are plotted for several popular inflationary models. The CMB 2σ bound $0.956 \leq n_s \leq 0.978$ and the upper bound on r , given in equation (2.15), are indicated by the two vertical and the horizontal brown dotted lines respectively. Predictions of the KKLT model, which we use as our base potential in this work, is shown by the red color curves.

Our speed-breaker is the local Gaussian bump

$$\varepsilon(\phi) = A \exp \left[-\frac{1}{2} \frac{(\phi - \phi_0)^2}{\sigma^2} \right], \quad (3.3)$$

which is characterised by its height A , position ϕ_0 and width σ (also see [66] for earlier application of a Gaussian bump).

The full potential in (3.1) therefore becomes

$$V(\phi) = V_0 \frac{\phi^2}{M^2 + \phi^2} \left[1 + A \exp \left(-\frac{1}{2} \frac{(\phi - \phi_0)^2}{\sigma^2} \right) \right]. \quad (3.4)$$

One notes that $V(\phi)$ is characterized by 4 parameters $\{V_0, A, \phi_0, \sigma\}$. Since V_0 fixes the overall CMB normalization only three parameters $\{A, \phi_0, \sigma\}$ are relevant for PBH formation. We will see that a speed-breaker consisting of a tiny bump of height $A \ll 1$ slows down the inflaton field sufficiently to enhance the scalar power spectrum relevant for PBH formation.

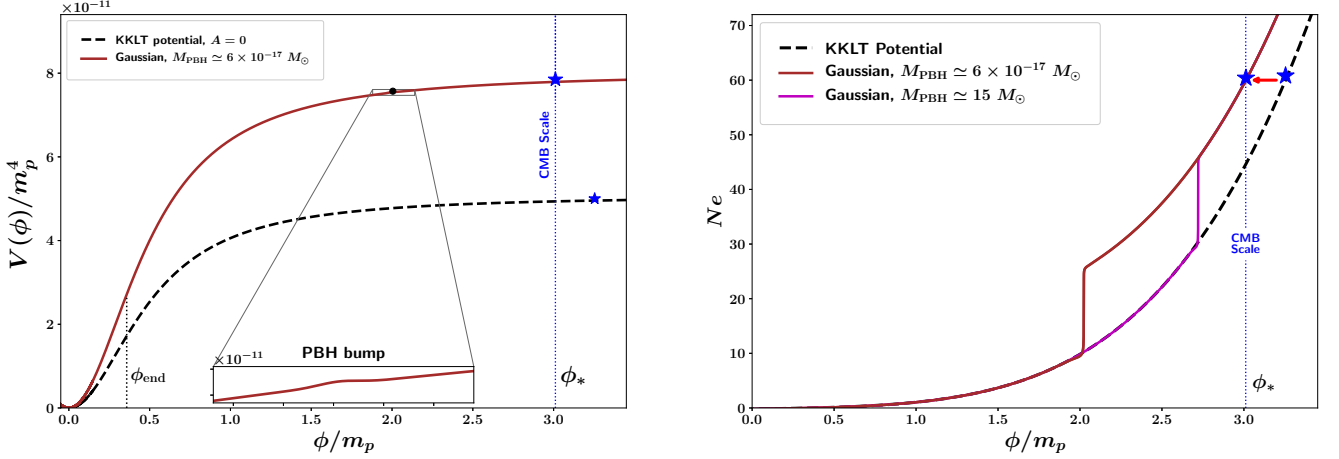


Figure 6: **Left panel:** shows KKLT potential with a small bump for PBH formation (3.4). The potential which gives rise to PBHs of mass $M_{\text{PBH}} \simeq 6 \times 10^{-17} M_{\odot}$ is shown by the brown color curve. The base potential is shown by the dashed black color curve. Black dot on the brown curve shows the bump location. The bump is not readily visible due to its small size and has been shown greatly amplified in the inset. **Right panel:** illustrates the enhancement in the number of e-foldings, with respect to the base potential, caused by bumps in the inflaton potential for PBHs of mass $M_{\text{PBH}} \simeq 6 \times 10^{-17} M_{\odot}$ and $M_{\text{PBH}} \simeq 15 M_{\odot}$ by the brown and the purple color curves respectively. The CMB pivot scale is shown by a blue star. Note that the CMB pivot scale ϕ_* gets shifted towards a smaller value for a potential with a bump as compared to the bump-free base potential. The parameters A, σ, ϕ_0 characterizing the bump have been chosen so that ϕ_* remains almost the same for all three cases given in table 1.

The parameter space of our model can accommodate the production of narrow band PBHs with a sharply peaked (almost monochromatic) mass function which ranges from the

microscopic $M_{\text{PBH}} \sim 10^{-18} M_{\odot}$ to the macroscopic $100 M_{\odot}$. We shall show explicit results for three distinct mass scales $M_{\text{PBH}} \simeq 6 \times 10^{-17} M_{\odot}$, $10^{-13} M_{\odot}$ and $15 M_{\odot}$. PBHs produced in each of these bins can contribute significantly to the total dark matter density in the universe. The parameter space relevant for producing PBHs of these masses is given in table 1. We would like to stress that the bumps in our potential are really tiny, since $A \ll 1$. Hence they are not readily discernible in the left panel of figure 6 and are shown greatly magnified in the inset. Their location is shown by black dots on the potential. Note also that the parameters A and σ need to be tuned to an accuracy of about two decimal places to ensure the desired abundance of PBHs. This is also discussed at the end of sec. 3.4.

It is important to mention that since we are essentially estimating M_{PBH} and the fractional PBH abundance f_{PBH} using $\{A, \phi_0, \sigma\}$, it is possible to come up with a multiple set of values of A , ϕ_0 and σ which result in roughly the same $\{M_{\text{PBH}}, f_{\text{PBH}}\}$. However all these different values of $\{A, \phi_0, \sigma\}$ will generally lead to different values of the pivot scale ϕ_* which, in turn, will lead to different values of n_s and r in the CMB. To avoid this ambiguity, we have chosen the parameters $\{A, \phi_0, \sigma\}$ in table 1 in such a way such that for different M_{PBH} the value of n_s and r at the CMB pivot scale remains unchanged, namely $n_s \simeq 0.965$, $r \simeq 0.0025$. This is reflected in figure 6 which shows that the CMB pivot scale value ϕ_* (blue star) is almost the same for both PBH cases⁶. Another way to think about this is by looking at the right panel of figure 6 which illustrates that the extra number of e-foldings ΔN_e due to the presence of the speed-breaker is roughly the same for both PBH cases. The fact that our parameter space allows us to achieve this is an important characteristic of our model. From table 1, we notice that by keeping ϕ_* (and hence n_s and r) almost fixed, the generation of higher mass PBHs requires the bump to be smaller in height A and sharper in width (smaller σ) while the location of the bump ϕ_0 moves closer to ϕ_* as M_{PBH} increases.

M_{PBH}	A	σ (in m_p)	ϕ_0 (in m_p)
$6 \times 10^{-17} M_{\odot}$	1.876×10^{-3}	1.993×10^{-2}	2.005
$1.04 \times 10^{-13} M_{\odot}$	1.17×10^{-3}	1.59×10^{-2}	2.188
$15.5 M_{\odot}$	3.502×10^{-4}	8.818×10^{-3}	2.713

Table 1: PBH parameters A , σ , ϕ_0 for our potential (3.4) are shown for three different PBH mass scales (determined using the Press-Schechter formalism). Note that the CMB pivot scale is $\phi_* \simeq 3 m_p$ and $n_s \simeq 0.965$, $r \simeq 0.0025$ for all three PBH mass values.

As discussed in section 2.1, a large amplification of $P_{\mathcal{R}}$ is obtained by slowing down the inflaton field by a PBH feature, which in this case is a local bump which acts like a speed-breaker. However the slow-roll condition (2.7) is violated during this large amplification of the scalar power spectrum. This is demonstrated in figure 2 for the case of $10^{-13} M_{\odot}$ PBH formation in our model. The right panel of this figure shows that the second slow-roll parameter $|\eta_H|$ becomes larger than $O(1)$ due to a sharp decrease in the value of ϵ_H near the location of the bump⁷. The slow-roll approximation (2.8), therefore underestimates the peak

⁶Note that in relation to ϕ_* for the bare potential, the value of ϕ_* for potentials with a bump shifts towards the left towards ϕ_{end} , as discussed earlier.

⁷Note that the transient phase when $|\eta_H|$ becomes nearly constant near its maximum value, shown in the

power and miscalculates the value of N_e^{PBH} and $P_{\mathcal{R}}$. The latter must therefore be determined by integrating the Mukhanov-Sasaki equation which gives a larger value of $P_{\mathcal{R}}$ as shown in the right panel of figure 4. Finally, $P_{\mathcal{R}}$, computed using the Mukhanov-Sasaki formalism is shown for all three bump locations in figure 7.

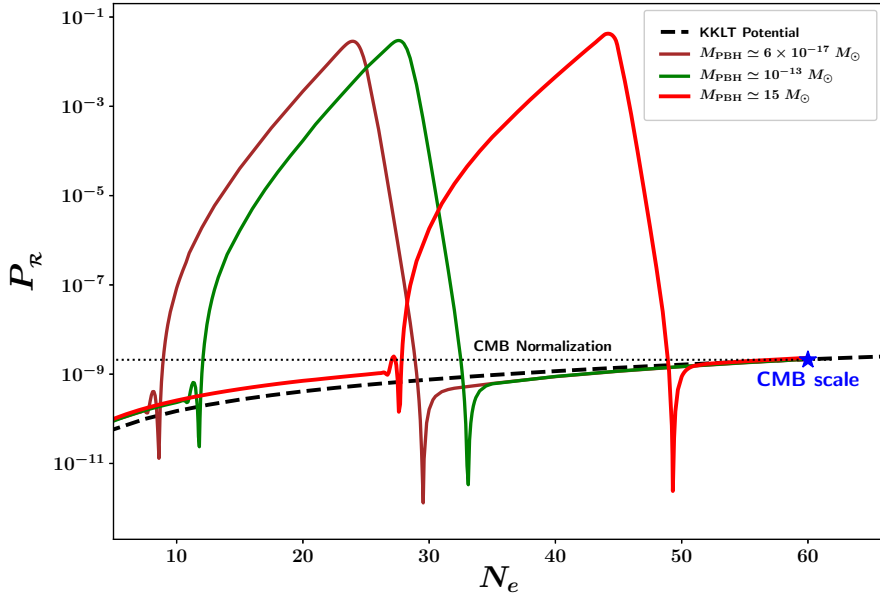


Figure 7: The scalar power spectrum $P_{\mathcal{R}}$ is plotted as a function of the number of e-foldings before the end of inflation, N_e . Note the enhancement in $\mathcal{P}_{\mathcal{R}}$ (computed using the Mukhanov-Sasaki formalism) in KKLT inflation (3.4) for three different PBH mass scales. In each case, $P_{\mathcal{R}}$ gets amplified by at least a factor of 10^7 with respect to the base potential (dashed black). The parameters A , σ , ϕ_0 , given in table 1, have been chosen to ensure the same value of n_s and r at the pivot scale (blue star), for the three bumps.

3.2 Primordial black holes from α -attractor Inflation

In order to demonstrate the versatility of our model, we turn to a different case where the base potential in (3.1) is associated with the T-Model⁸ of α -attractors [54, 55]

$$V_b(\phi) = V_0 \tanh^{2n} \left(\frac{\phi}{\sqrt{6\alpha} m_p} \right), \quad (3.5)$$

where V_0 fixes the overall CMB normalization given by equations (2.8) & (2.16). The n_s and r values of the base potential are shown in green color in figure 5 for $n = 1$. Although the base potential (3.5) has two free parameters α and n , we shall set $\alpha = 1$ and $n = 1$, for

right panel of figure 2, corresponds to the case of constant-roll inflation [67]. See [68] for PBH formation in the context of constant-roll inflation.

⁸One could also use the asymptotically flat wing of the E-Model of α -attractors, which in the case of $\alpha = 1$, resembles the potential for Starobinsky inflation [69] in the Einstein frame.

simplicity. Our speed-breaker⁹ is given by a local hyperbolic bump of the form

$$\varepsilon(\phi) = A \cosh^{-2} \left(\frac{\phi - \phi_0}{\sigma} \right) , \quad (3.6)$$

which is characterised by its height A , position ϕ_0 and width σ , as in the case of the Gaussian bump in (3.3).

The full potential in (3.1) therefore becomes

$$V(\phi) = V_0 \tanh^2 \left(\frac{\phi}{\sqrt{6\alpha} m_p} \right) \left[1 + A \cosh^{-2} \left(\frac{\phi - \phi_0}{\sigma} \right) \right] . \quad (3.7)$$

One notes that $V(\phi)$ is characterized by 4 parameters $\{V_0, A, \phi_0, \sigma\}$. Since V_0 fixes the overall CMB normalization only three parameters $\{A, \phi_0, \sigma\}$ are relevant for PBH formation. Table 2 demonstrates that a speed-breaker consisting of a tiny bump of height $A \ll 1$ slows down the inflaton field sufficiently to enhance the scalar power spectrum relevant for PBH formation¹⁰.

M_{PBH}	A	σ (in m_p)	ϕ_0 (in m_p)
$5.7 \times 10^{-17} M_\odot$	3.032×10^{-3}	3.058×10^{-2}	4.6
$1.14 \times 10^{-13} M_\odot$	2.045×10^{-3}	2.525×10^{-2}	4.85
$14.7 M_\odot$	6.401×10^{-4}	1.429×10^{-2}	5.58

Table 2: PBH parameters A , σ , ϕ_0 for our potential (3.7) are shown for three different PBH mass scales (determined using the Press-Schechter formalism). Note that the CMB pivot scale is $\phi_* \simeq 6 m_p$ and $n_s \simeq 0.96$, $r \simeq 0.0047$ for all three PBH mass values.

As discussed before, the parameter space of our model can accommodate the production of narrow band PBHs with a sharply peaked (almost monochromatic) mass function which ranges from the microscopic $M_{\text{PBH}} \sim 10^{-18} M_\odot$ to the macroscopic $100 M_\odot$. As in the case of the KKLT potential with a Gaussian bump (3.4), we show our results for the α -attractor potential with a hyperbolic bump (3.7) for three distinct mass scales $M_{\text{PBH}} \simeq 6 \times 10^{-17} M_\odot$, $10^{-13} M_\odot$ and $15 M_\odot$. The parameter space relevant for producing PBHs of these masses is given in table 2. The parameters have been chosen to ensure the same value of n_s and r at the CMB pivot scale, namely $n_s \simeq 0.96$, $r \simeq 0.0047$. We would again like to highlight the fact that the bumps in our potential are really tiny since $A \ll 1$. Note also that the parameters A and σ need to be tuned to an accuracy of more than two decimal places to ensure the desired abundance of PBHs as previously discussed. The scalar power spectrum $\mathcal{P}_{\mathcal{R}}$ (computed using the Mukhanov-Sasaki formalism) is shown in figure 8 for three different PBH mass scales while the abundance of PBHs is shown in figure 14.

⁹Note that our results are not very sensitive to the precise form of the speed-breaker bump. We use the bump (3.6) simply because both bump (3.6) and base potential (3.5) are given in terms of hyperbolic functions. The Gaussian speed-breaker (3.3) in tandem with the α -attractor potential (3.5) would have given similar results.

¹⁰See [70, 71] for PBH formation in near inflection point models constructed from α -attractor potentials.

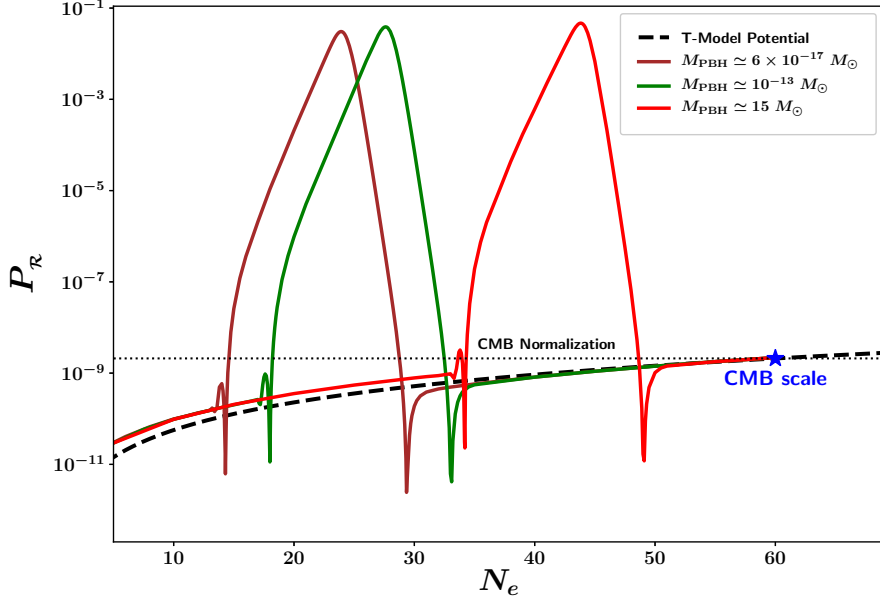


Figure 8: The scalar power spectrum $P_{\mathcal{R}}$ is plotted as a function of the number of e-foldings before the end of inflation, N_e . Note the enhancement in $\mathcal{P}_{\mathcal{R}}$ (computed using the Mukhanov-Sasaki formalism) in α -attractor inflation (3.7) for three different PBH mass scales. In each case, $P_{\mathcal{R}}$ gets amplified by at least a factor of 10^7 with respect to the base potential (dashed black). The parameters A , σ , ϕ_0 , given in table 2, have been chosen to ensure the same value of n_s and r at the pivot scale (blue star), for the three bumps.

3.3 Primordial black holes from a dip in the inflaton potential

It is interesting that our model for PBH formation also works if the bump in (3.1) is replaced by a dip so that

$$V(\phi) = V_b(\phi) [1 - \varepsilon(\phi)] \quad (3.8)$$

where V_b is the base inflationary potential responsible for generating quantum fluctuations compatible with the CMB constraints on n_s , r . The term $\varepsilon(\phi) \ll 1$ describes a tiny dip in the potential at ϕ_0 having width σ .

Consequently a general form for the potential containing a tiny bump/dip is

$$V(\phi) = V_b(\phi) [1 \pm \varepsilon(\phi)] \quad , \quad (3.9)$$

with the ‘+’ sign corresponding to a bump and a ‘−’ sign to a dip; see figure 9.

We illustrate the possibility that a dip can lead to PBH formation by superimposing a Gaussian dip on a base KKLT potential so that

$$V(\phi) = V_0 \frac{\phi^2}{M^2 + \phi^2} \left[1 - A \exp \left(-\frac{1}{2} \frac{(\phi - \phi_0)^2}{\sigma^2} \right) \right] \quad . \quad (3.10)$$

The Gaussian dip parameters for $M_{\text{PBH}} \simeq 10^{-13} M_{\odot}$ are listed in the second row of table 3 while the first row corresponds to parameters for a Gaussian bump. The behaviour of

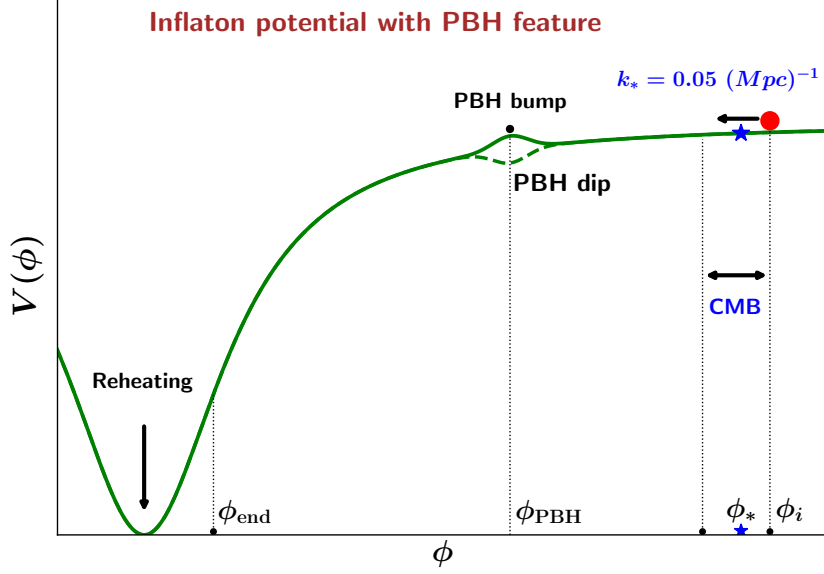


Figure 9: This figure schematically shows the base potential with a PBH feature in the form of either a tiny local bump or a tiny local dip superimposed on it. The feature arises at an intermediate scalar field value ϕ_{PBH} before the end of inflation ϕ_{end} . Note that the bump/dip size is shown significantly amplified for the purposes of illustration.

slow-roll parameters ϵ_H and η_H is shown in figure 10 which indicates that $|\eta_H|$ can grow to become of order unity, due to slowing down of the inflaton field while climbing out of the local minimum, thereby violating the slow-roll condition (2.7), as shown earlier for a tiny bump in the right panel of figure 2.

PBH feature	A	σ (in m_p)	ϕ_0 (in m_p)
Bump	1.17×10^{-3}	1.59×10^{-2}	2.188
Dip	2.205×10^{-3}	2.742×10^{-2}	2.175

Table 3: Parameters A , σ , ϕ_0 which generate PBHs of mass $M_{\text{PBH}} \simeq 10^{-13} M_\odot$ for KKLT inflation (3.2) with a local Gaussian feature (3.3) & (3.9) are listed. The first and the second rows indicate the parameters corresponding a tiny local bump/dip respectively.

A large amplification of $P_{\mathcal{R}}$ arises when the inflaton field slows down while climbing up the dip, away from its local minimum. As for a bump, the slow-roll condition (2.7) is violated during this large amplification of the scalar power spectrum, and $P_{\mathcal{R}}$ must therefore be determined by integrating the Mukhanov-Sasaki equation for a dip. The resulting power spectrum corresponding to the formation PBH's of mass of $10^{-13} M_\odot$ is shown in figure 11. From this figure it is clear that the power amplification required to form PBHs of mass

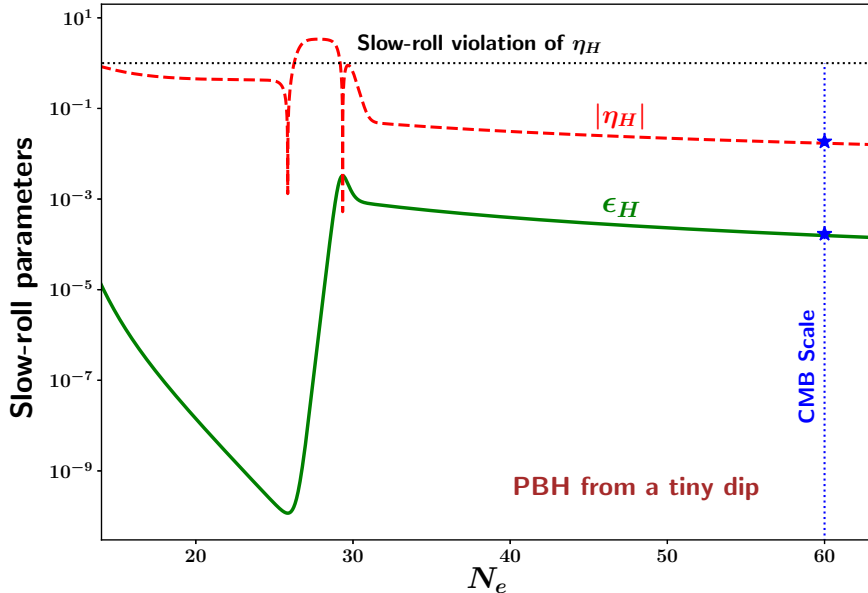


Figure 10: This figure demonstrates the violation of the slow-roll conditions (2.7) during the formation of $10^{-13} M_{\odot}$ PBHs due to the presence of a feature in the form of a Gaussian dip in the base KKLT potential (3.10).

$M_{\text{PBH}} \simeq 10^{-13} M_{\odot}$ from a local dip (dashed red) is similar to that obtained from a bump (solid green).

While we have explicitly described the power amplification required to form $10^{-13} M_{\odot}$ PBHs, one can easily generate PBHs in the mass range $10^{-17} M_{\odot} \leq M_{\text{PBH}} \leq 100 M_{\odot}$ using a tiny local dip as in the case of a tiny local bump. We therefore conclude that PBHs of mass $10^{-17} M_{\odot} \leq M_{\text{PBH}} \leq 100 M_{\odot}$ can be generated using a tiny local feature in the form of a bump or a dip as a local correction to the base inflationary potential modelled by the general form (3.9).

Before moving forward to discuss the mass function of PBHs, we would like to emphasize that while we have explicitly demonstrated the amplification of the scalar power spectrum due to a local Gaussian bump/dip superimposed on a base KKLT potential as well as a local hyperbolic bump/dip superimposed on the α -attractor potential, the choice of bump/dip need not be restricted to these two examples. In fact our model is quite robust and works for any local bump/dip superimposed on an asymptotically flat base potential.

3.4 Formation and abundance of primordial black holes

PBHs are usually characterized by their mass M_{PBH} and abundance f_{PBH} . When a large fluctuation mode, generated during inflation on some scale $k = k_{\text{PBH}}$, re-enters the Hubble radius i.e., $k = aH$ it can form a PBH with a mass specific to the mode k_{PBH} and a dependence on the Hubble scale H during re-entry. The abundance of PBHs therefore depends both upon the value of k_{PBH} and on the amplified power spectrum $P_{\mathcal{R}}$. The amplification of short wavelength modes discussed in the previous section translates into the formation of PBHs during the radiation dominated epoch after reheating, as shown in figure 3.

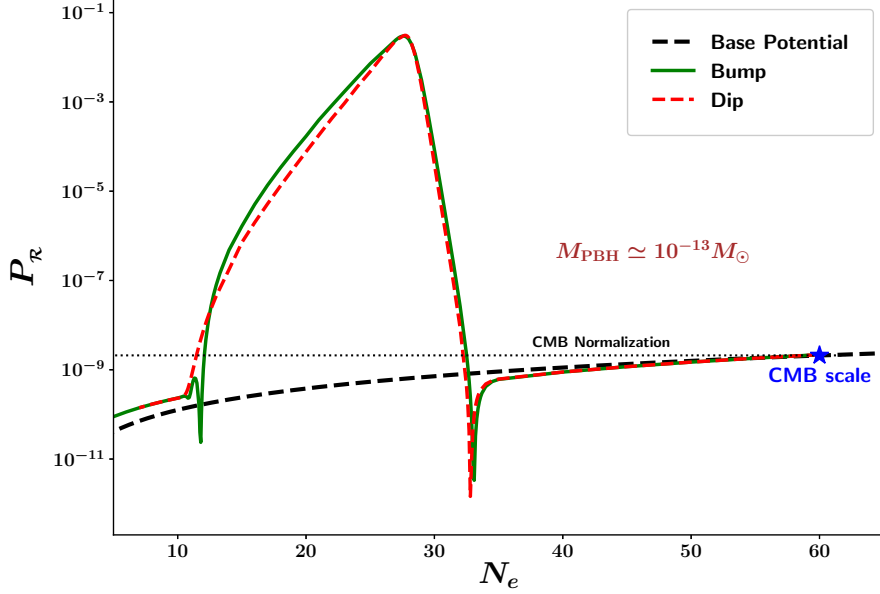


Figure 11: The scalar power spectrum $P_{\mathcal{R}}$ (computed using the Mukhanov-Sasaki formalism) is plotted as a function of the number of e-foldings before the end of inflation, N_e , for the case of $10^{-13} M_{\odot}$ PBHs which form because of the presence of a local Gaussian bump/dip superimposed on the base KKLT potential. Note that an almost identical amplification of power is obtained using a bump (solid green) or dip (dashed red). The parameters describing the Gaussian bump/dip are listed in table 3.

Mass of primordial black holes

The mass of a newly formed black hole is related to the Hubble mass at formation and is given by [38, 48]

$$M_{\text{PBH}} = \gamma M_{\text{H}} = \gamma \frac{4\pi m_p^2}{H}, \quad (3.11)$$

where γ is the efficiency of collapse, assumed to be $\gamma = 0.2$ for PBH formation in the radiative epoch [4, 25, 38]. The Hubble scale in the radiative epoch can be written as (see appendix B, [48])

$$H^2 = \Omega_{0r} H_0^2 (1+z)^4 \left(\frac{g_*}{g_{0*}} \right)^{-1/3} \left(\frac{g_{0*}^s}{g_{0*}} \right)^{4/3}, \quad (3.12)$$

where $g_{0*} = 3.38$ and $g_{0*}^s = 3.94$ are the effective energy and entropy degrees of freedom at the present epoch, while the relativistic degrees of freedom of the energy density in the radiation dominated epoch during the formation of PBHs correspond to $g_* \simeq 106.75$. The radiation density parameter at the present epoch is $\Omega_{0r} h^2 = 4.18 \times 10^{-5}$. We therefore obtain the following expressions for the mass of a newly formed PBH (see appendix B, [25, 38, 48, 49])

$$\frac{M_{\text{PBH}}}{M_{\odot}} = 1.55 \times 10^{24} \left(\frac{\gamma}{0.2} \right) \left(\frac{g_*}{106.75} \right)^{1/6} (1+z)^{-2}, \quad \text{equivalently} \quad (3.13)$$

$$\frac{M_{\text{PBH}}}{M_{\odot}} = 1.13 \times 10^{15} \left(\frac{\gamma}{0.2} \right) \left(\frac{g_*}{106.75} \right)^{-1/6} \left(\frac{k_{\text{PBH}}}{k_*} \right)^{-2}. \quad (3.14)$$

Expression (3.13) suggests that PBH forming at an earlier epoch have a smaller mass compared to those that formed later. Solar mass PBHs are formed at redshifts of about 10^{12} whereas smaller mass PBHs can form at much higher redshifts. After their formation, the PBH density redshifts just like pressureless matter until the present epoch (ignoring merger events and accretion). Hence PBHs behave just like dark matter for a substantial part of the cosmic history. Similarly expression (3.14) infers that solar mass PBHs are formed when a large fluctuation mode with comoving wave number $k_{\text{PBH}} \simeq 10^7 k_*$ enters the Hubble radius. M_{PBH} can also be related to the number of e-foldings before the end of inflation, N_e^{PBH} by the relation (appendix B, [48])

$$N_* - N_e^{\text{PBH}} = 17.33 + \frac{1}{2} \ln \frac{\gamma}{0.2} - \frac{1}{12} \ln \frac{g_*}{106.75} - \frac{1}{2} \ln \frac{M_{\text{PBH}}}{M_{\odot}}, \quad (3.15)$$

which indicates that a large fluctuation mode corresponding to solar mass black holes must exit the Hubble scale about 17 e-foldings after the exit of the CMB pivot scale. Figure 12 shows the Hubble exit e-fold number for modes corresponding to different PBH mass scales. In this work we focus on 3 distinct PBH mass scales: $6 \times 10^{-17} M_{\odot}$, $10^{-13} M_{\odot}$, $15 M_{\odot}$. PBHs belonging to these bins can contribute substantially to the present dark matter density and also play an important role in different astrophysical processes.

Abundance of primordial black holes

As stated before, primordial over densities caused by horizon re-entry of modes with significantly amplified $P_{\mathcal{R}}$ collapse to form primordial black holes. The fractional abundance of PBHs at the present epoch is defined as

$$f_{\text{PBH}}^{\text{tot}} = \int \frac{dM_{\text{PBH}}}{M_{\text{PBH}}} f_{\text{PBH}}(M_{\text{PBH}}), \quad (3.16)$$

where the mass function of fractional abundance of PBHs, defined as

$$f_{\text{PBH}} = \frac{\Omega_{0\text{PBH}}(M_{\text{PBH}})}{\Omega_{0\text{DM}}}, \quad (3.17)$$

is given by (see appendix B, [38])

$$f_{\text{PBH}}(M_{\text{PBH}}) = 1.68 \times 10^8 \left(\frac{\gamma}{0.2} \right)^{1/2} \left(\frac{g_*}{106.75} \right)^{-1/4} \left(\frac{M_{\text{PBH}}}{M_{\odot}} \right)^{-1/2} \beta(M_{\text{PBH}}). \quad (3.18)$$

Where the mass fraction $\beta(M_{\text{PBH}})$ of PBHs at formation is defined by

$$\beta(M_{\text{PBH}}) = \frac{\rho_{\text{PBH}}}{\rho_{\text{tot}}} \Big|_{\text{formation}}. \quad (3.19)$$

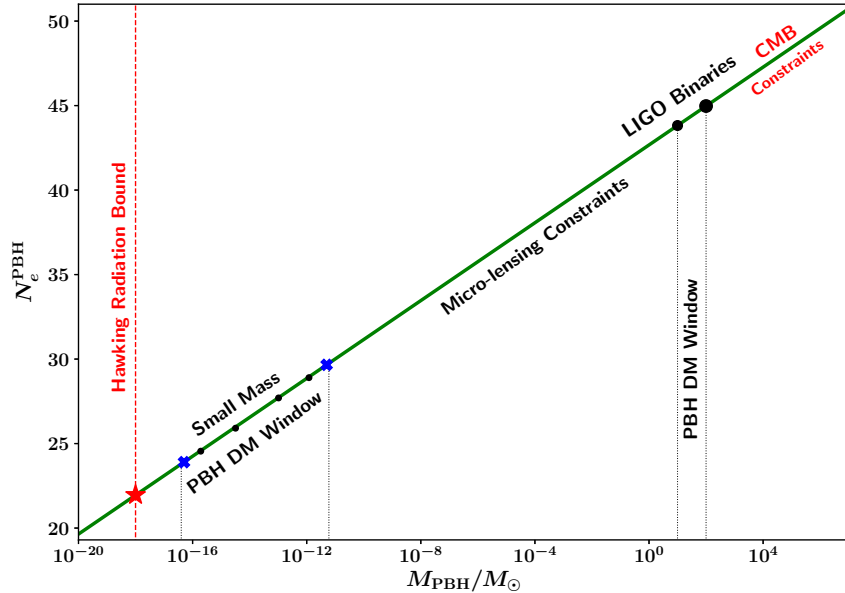


Figure 12: This figure describes the relation between two important quantities: (i) the number of e-foldings N_e^{PBH} before the end of inflation when a given fluctuation mode exits the Hubble radius, and (ii) the mass of PBHs formed upon the re-entry of that mode. PBHs with different masses are constrained by different sets of observations [38]. PBHs of mass less than $10^{-18} M_\odot$ evaporate by Hawking radiation and do not survive until the present epoch. For PBHs to form a significant fraction of dark matter density today, i.e. $f_{\text{PBH}} \geq 0.1$, they should lie in the mass windows $M_{\text{PBH}} \sim 6 \times 10^{-17} M_\odot$, $10^{-13} M_\odot$, $15 M_\odot$ [38, 72, 73].

Since $\beta(M_{\text{PBH}})$ can be calculated from the primordial power spectrum $P_{\mathcal{R}}$ in the Press-Schechter formalism¹¹, one can in principle estimate the mass function for the fractional abundance of PBHs for a given inflationary model in the following way.

In the Press-Schechter formalism [77], the mass fraction of PBHs at formation $\beta(M_{\text{PBH}})$ for a given mass is defined as the probability that the Gaussian density contrast (or equivalently the Gaussian comoving curvature perturbation \mathcal{R} or ζ), coarse-grained over the comoving Hubble scale $R = 1/k_{\text{PBH}} = 1/(aH)_{\text{PBH}}$ by a suitable window function, is larger than the threshold δ_{th} (or ζ_{th}) for PBH formation and is therefore expressed as [25, 38, 74, 78]

$$\beta(M_{\text{PBH}}) = \gamma \int_{\delta_{\text{th}}}^1 P(\delta) d\delta, \quad (3.20)$$

¹¹Note that one can also compute $\beta(M_{\text{PBH}})$ using the peak theory formalism where the primordial overdensity condition is stated in terms of the peak value of a fluctuation mode, as opposed to the average value used in Press-Schechter theory. Both the formalisms predict the same range for M_{PBH} for a narrow-band/monochromatic mass function $f_{\text{PBH}}(M_{\text{PBH}})$, while the peak value of $\beta(M_{\text{PBH}})$ (and hence of $f_{\text{PBH}}(M_{\text{PBH}})$) is usually higher in the peak theory formalism [74–76].

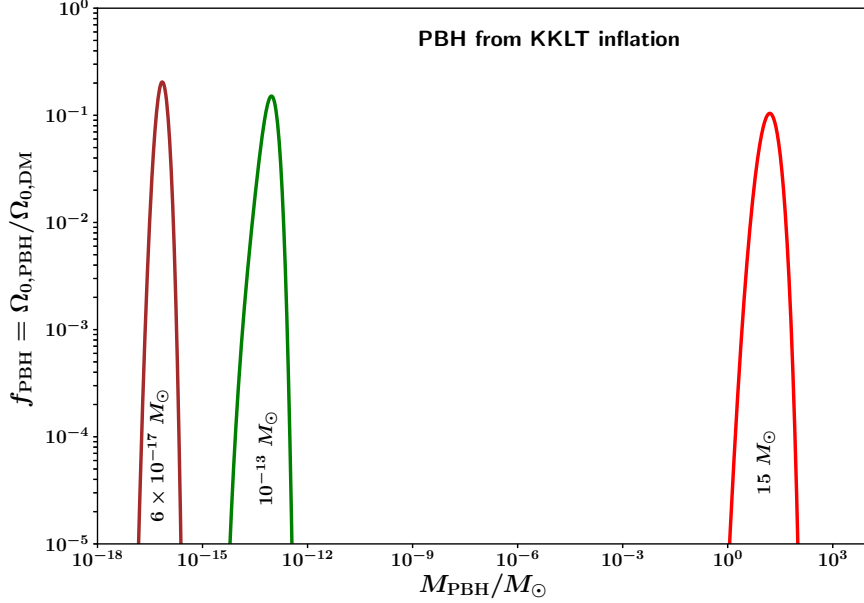


Figure 13: The fractional abundance of PBHs, given by equation (3.18), is shown as a function of PBH mass in the KKLT model (3.4) for the three bumps considered in table 1. One sees that KKLT inflation with a tiny bump can generate nearly monochromatic narrow band mass functions, corresponding to 6×10^{-17} , 10^{-13} and $15 M_\odot$ black holes with $f_{\text{PBH}} \geq 0.1$. PBHs in these bands can therefore contribute significantly to the dark matter density in the universe today.

which is given by

$$\beta(M_{\text{PBH}}) = \gamma \int_{\delta_{\text{th}}}^1 \frac{d\delta}{\sqrt{2\pi}\sigma_{M_{\text{PBH}}}} \exp\left[-\frac{\delta^2}{2\sigma_{M_{\text{PBH}}}^2}\right] \approx \gamma \frac{\sigma_{M_{\text{PBH}}}}{\sqrt{2\pi}\delta_{\text{th}}} \exp\left[-\frac{\delta_{\text{th}}^2}{2\sigma_{M_{\text{PBH}}}^2}\right]. \quad (3.21)$$

The variance of the density contrast coarse-grained over the comoving Hubble scale $R = 1/k_{\text{PBH}} = 1/(aH)_{\text{PBH}}$ (or mass scale M_{PBH}) is given by

$$\sigma_{M_{\text{PBH}}}^2 = \int \frac{dk}{k} P_\delta(k) W^2(k, R), \quad (3.22)$$

where $W(k, R)$ is the Fourier transform of the Gaussian window function used for smearing the original Gaussian density contrast field over the comoving Hubble scale to obtain the coarse-grained density contrast δ and is given by [25, 74]

$$W(k, R) = \exp\left(-\frac{1}{2}k^2 R^2\right). \quad (3.23)$$

The power spectrum for the density contrast P_δ is related, in the radiation dominated epoch, to the primordial comoving curvature power spectrum by the famous expression [79]

$$P_\delta(k) = \frac{16}{81} \left(\frac{k}{aH}\right)^4 P_{\mathcal{R}}(k). \quad (3.24)$$

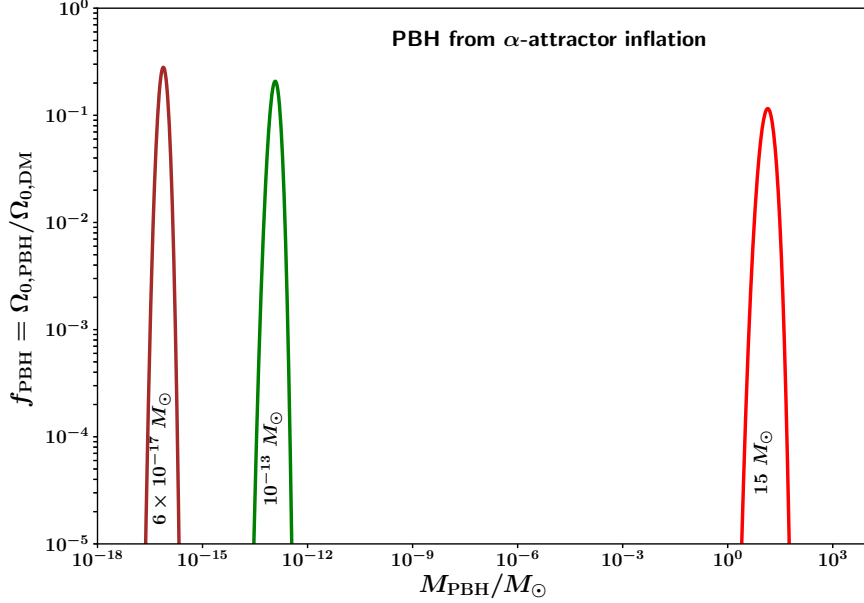


Figure 14: The fractional abundance of PBHs, given by equation (3.18), is shown as a function of PBH mass in the α -attractor model (3.7) for the three bumps considered in table 2. One sees that α -attractor inflation with a tiny bump can generate nearly monochromatic narrow band mass functions, corresponding to 6×10^{-17} , 10^{-13} and $15 M_\odot$ black holes with $f_{\text{PBH}} \geq 0.1$. PBHs in these bands can therefore contribute significantly to the dark matter density in the universe today.

From expressions (3.22), (3.23) and (3.24), and using the fact that $R = 1/k_{\text{PBH}} = 1/(aH)_{\text{PBH}}$ we get a final expression for the variance of the density contrast as

$$\sigma_{M_{\text{PBH}}}^2 = \frac{16}{81} \int \frac{dk}{k} \left(\frac{k}{k_{\text{PBH}}} \right)^4 \exp \left(-\frac{k^2}{k_{\text{PBH}}^2} \right) P_{\mathcal{R}}(k). \quad (3.25)$$

Substituting equations (3.21) and (3.25) in (3.18), one can compute the mass dependent fractional PBH abundance $f_{\text{PBH}}(M_{\text{PBH}})$ within the framework of the Press-Schechter formalism. There are several caveats which need to be borne in mind before proceeding to apply the techniques discussed above to our inflationary potential. First of all, equation (3.21) suggests that f_{PBH} strongly depends on the value of δ_{th} , as illustrated in figure 15. However there have been several detailed investigations, both analytical as well as numerical, which suggest that the numerically allowed value of the threshold may be rather broad with δ_{th} ranging from 0.3 till 0.66 for PBH formation in the radiation dominated epoch [3, 72, 78, 80–84]. The threshold value of density contrast in this work is assumed to be $\delta_{\text{th}} = 0.414$ which is supported by the analytical calculations of [78].

A second important thing to keep in mind is that since $\sigma_{M_{\text{PBH}}}$ depends upon the primordial power spectrum, f_{PBH} is quite sensitive to the peak value of $P_{\mathcal{R}}$ and hence a fine tuning of parameters of the inflationary potential upto a couple of decimal places is required in order to produce the desired abundance of PBHs. This is a generic requirement for PBH formation

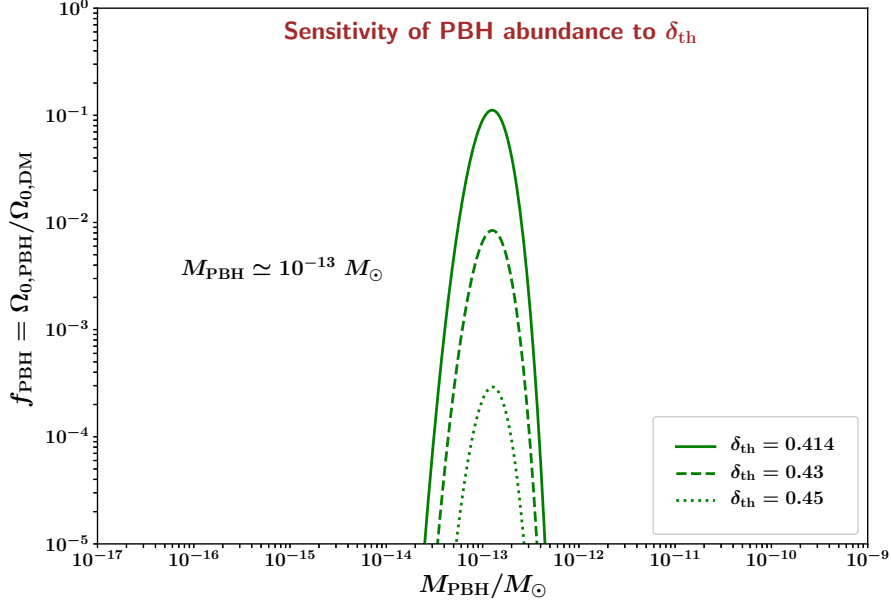


Figure 15: This figure highlights the strong dependence of the fractional abundance of PBHs, calculated in the framework of Press-Schechter formalism, on the threshold density contrast δ_{th} for a given primordial power spectrum $P_{\mathcal{R}}(k)$. We demonstrate this by showing $P_{\mathcal{R}}(k)$ determined by a bump-like feature which generates $10^{-13} M_{\odot}$ PBH's, as discussed in section 3 .

in the case of a monochromatic mass fraction and hence not specific to any particular model considered in the literature, as pointed out in [49, 50]. Also note that in this work we stick to the Press-Schechter formalism for the case of a monochromatic mass fraction $\beta(M_{PBH})$ due to the very narrow band mass range of the produced PBHs. PBH abundance for an extended mass function is described in [72, 73]. Another source of ambiguity in the computation of PBH abundance may come from the choice of the window function in equation (3.22). Although we use the popular Gaussian window (3.23), other window functions have been discussed in the literature and their effect on PBH abundance has been thoroughly investigated in [85, 86].

Keeping in mind these caveats, we now apply the methodology discussed in section 2.1 and 3.4 to our inflationary potential and compute the corresponding PBH mass function. It is important to mention that several interesting models have been proposed in the literature [25, 47, 49, 50] to produce PBHs in the cosmologically interesting mass range shown in figure 12. However it has also been noticed that in most models incorporating a near inflection point feature to generate PBH [47, 49, 50] the production of higher mass PBHs usually results in a high value of n_s which is in tension with the 2σ bound from CMB observations [60]. This problem can be traced to the fact that the PBH feature generated on a scale ϕ_{PBH} (see the right panel of figure 1) sensitively affects the CMB scale ϕ_* . In fact the higher the PBH mass the more red-tilted is n_s and hence the larger is its deviation from the CMB 2σ bound. Hence inflection point features in $V(\phi)$ can successfully account for relatively low mass PBH,

with $M_{\text{PBH}} \ll M_{\odot}$, for which ϕ_{PBH} lies very close to ϕ_{end} and does not affect ϕ_* .

This problem does not arise in our model since our bump-like/dip-like features in $V(\phi)$ appears locally and its location does not significantly affect the CMB spectral tilt n_s . Hence heavy primordial black holes can be produced with the same ease as light ones. Additionally, the functional form of the potential proposed in this work (3.1) has a simple structure in the form of a base inflationary potential V_b , responsible for generating the CMB observables n_s and r , and a local bump or dip superimposed on V_b to generate PBHs. In our view this scheme is simpler than most of the models proposed in the literature in which the PBH feature and the CMB observable part of the inflationary potential implicitly intermingle in a polynomial form for $V(\phi)$. Therefore, within our framework (3.9), namely

$$V(\phi) = \text{base potential} \pm \text{local correction}, \quad (3.26)$$

it becomes easier to consider CMB observables associated with the base potential $\{n_s, r, A_s\}$ and PBH observables $\{M_{\text{PBH}}, f_{\text{PBH}}\}$ associated with the bump or dip, separately.

The fractional abundance of primordial black holes $f_{\text{PBH}}(M_{\text{PBH}})$ in our model, corresponding to parameter values given in table 1, has been plotted in figure 13 (using the Press-Schechter formalism) and is consistent with current observational constraints [38, 87]. To determine the abundance accurately, we have obtained the primordial power spectrum $P_{\mathcal{R}}$ by solving the Mukhanov-Sasaki equation rather than using the slow-roll approximation. Our analysis indicates that it is possible to generate PBHs that can constitute a significant fraction of the dark matter density today. One might mention that $\sim 15 M_{\odot}$ PBHs could have additional significance in the context of binary black hole formation relevant to the LIGO/Virgo/KAGRA band [21, 38]. It is also interesting that the formation of PBHs in the mass range 10^{-13} – $10^{-12} M_{\odot}$, which is a window for PBH dark matter, inevitably leads to the generation of second order gravitational waves with frequency peaked in the mHz range – coincidentally the maximum sensitivity of the LISA mission [88]. This would be an interesting issue for further study.

An interesting feature of the power spectrum shown in figures 7, 8 and 11 is the presence of a dip in the power spectrum just prior to its amplification. The presence of such a dip was analytically established in [41] and has recently been noticed numerically in several studies [47, 49–51, 71] and appears to be a generic feature in all inflationary models in which an attractor slow-roll phase transitions to a non-attractor constant-roll phase with $\eta_H > \frac{3}{2}$. A thorough explanation of the dip was provided in [89, 90].

4 Discussion

Primordial black holes can play an extremely important role in different astrophysical and cosmological processes. While CMB observations do give us important information about the early stages of inflation by constraining the form of the inflaton potential near the CMB pivot scale, a large portion of the inflationary potential, corresponding to the last 50 e-foldings of expansion, remains virtually inaccessible to CMB observations. PBHs provide a natural tool with which this gap can be filled and lower scale physics can be studied. In particular PBHs can be used to probe the last few e-foldings of inflation. In fact even the non-detection of PBHs on a given mass scale can constrain models of the early universe [38]. Aside from probing the small scale part of the primordial power spectrum, PBHs may also contribute significantly to the present dark matter density of the universe. They might also seed the

formation of supermassive BHs and produce the black hole binaries that are relevant for the gravitational waves detections by LIGO and Virgo.

The Inflationary paradigm presents a natural playground for PBH model building. In these models, large fluctuation modes that leave the Hubble radius during inflation lead to PBH formation upon their re-entry, due to the gravitational collapse of correspondingly large fluctuations in the radiation+matter field. In canonical single field models of inflation, a feature in the form of a near inflection point can amplify the primordial fluctuations by several orders of magnitude favouring PBH formation. However attempts to produce larger than solar mass PBHs in these models adversely affect the scalar spectral tilt n_s , making it more red and in conflict with the 2σ CMB bound.

In this work we propose a simple phenomenological inflationary potential in which a tiny local bump is superimposed on top of a base potential. The bump acts like a speed breaker for the inflaton and slows it down. This leads to a large enhancement in the amplitude of scalar perturbations and results in PBH formation on the scale of the bump. The simple form of our potential allows one to consider CMB scale observables n_s & r and PBH scale physics, separately. Thus our model can generate PBHs on a variety of important physical scales ranging from the tiny $10^{-17} M_\odot$ to the super-solar $100 M_\odot$. Interestingly, upon fixing the CMB scale values of n_s and r for a given base potential, smaller and sharper bumps located closer to the pivot scale result in higher mass black holes. While we have explicitly demonstrated PBH formation for two important Inflationary scenario's namely KKLT inflation and an α -attractor model, we believe that our 'base + bump' approach may have a larger range of applicability, and work for other asymptotically flat base potentials as well. Indeed, we feel that our analysis should be valid for any generically tiny local dip/bump-like feature superimposed on a base inflationary potential.

The reader should note that since our approach in this paper is largely phenomenological, we do not provide a firm theoretical basis for any given form of a bump/dip in this paper. However, the possibility that a tiny bump/dip could appear as a small local radiative correction to the base potential remains an open question worthy of future examination.

One might mention that the standard method of calculating the abundance f_{PBH} of primordial black holes at the present epoch, which we use here (as described in appendix B), is based upon the assumption that the mass of PBHs remains unchanged until the present epoch. However M_{PBH} may grow in the early universe either through accretion or by merger events, which would lead to a transfer of mass from low to high mass PBHs. This could be particularly important for heavy PBHs which might seed the formation of supermassive black holes in the nuclei of galaxies and AGN's [12, 13, 91]. We shall revert to some of these issues in a future work.

It is interesting to note that since cosmologically abundant PBH formation requires the primordial power spectrum to be as large as $P_{\mathcal{R}} \approx 10^{-2}$, higher order quantum fluctuations in the comoving curvature perturbation \mathcal{R} (equivalently curvature perturbation on uniform density hypersurfaces ζ) may become important, and this could have interesting consequences for primordial gravitational wave (GW) generation. In fact it has been shown [92] that a spectrum of second order GWs can be generated from first order scalar fluctuations. Thus an important future direction of study might be the effect of higher order non-linear scalar fluctuations on primordial GWs [88, 93–96]. Interestingly, the sharp-drop in the speed of the inflaton, that leads to power amplification for PBH formation, also tends to increase the quantum diffusion of the inflaton field with respect to classical roll-down. This process also needs to be taken into account for a more accurate determination of the PBH mass function

[97–99]. Finally note that while we have assumed Gaussian comoving curvature perturbations for estimating the abundance of PBHs, the effect of non-Gaussianities in the primordial fluctuations may also be important for PBH formation, as discussed in [33, 66, 100–106]. We propose to revisit some of these issues in a future work.

Acknowledgments

S.S.M. thanks the Council of Scientific and Industrial Research (CSIR), India, for financial support as senior research fellow. V.S is partially supported by the J.C.Bose Fellowship of Department of Science and Technology, Government of India. S.S.M would like to thank Surya Narayan Sahoo for technical help in some of the numerical work and Surhud More for discussions on observational constraints on primordial black holes. SSM also thanks L. Sriramkumar, H.V. Ragavendra, Michele Oliosi and Takahiro Tanaka for useful discussions regarding modelling of primordial black holes as well as Vincent Vennin for discussions on possible implications of quantum diffusion.

A The Mukhanov-Sasaki Equation

In the standard scenario of a minimally coupled single canonical scalar field ϕ as inflaton, two gauge independent massless fields, one scalar and one transverse traceless tensor, get excited during inflation and receive quantum fluctuations correlated over super-Hubble scales [107] at late times. The evolution of the scalar degree of freedom called the comoving curvature perturbation \mathcal{R} (which is also related to the curvature perturbation on uniform-density hypersurfaces ζ and both are equal on super-Hubble scales $k \ll aH$) is described by the following second order action [57]

$$S_{(2)}[\mathcal{R}] = \frac{1}{2} \int d^4x \, a^3 \frac{\dot{\phi}^2}{H^2} \left[\dot{\mathcal{R}}^2 - \frac{1}{a^2} (\partial_i \mathcal{R})^2 \right], \quad (\text{A.1})$$

which upon the change of variable

$$v \equiv z\mathcal{R}, \quad \text{with} \quad z = am_p \sqrt{2\epsilon_H} = a \frac{\dot{\phi}}{H}, \quad (\text{A.2})$$

takes the form

$$S_{(2)}[v] = \frac{1}{2} \int d^4x \left[(v')^2 + (\partial_i v)^2 + \frac{z''}{z} v^2 \right], \quad (\text{A.3})$$

where the $(')$ denotes derivative with respect to conformal time τ . The variable v , which itself is a scalar quantum field like \mathcal{R} , is called the Mukhanov-Sasaki variable in the literature and its Fourier modes v_k satisfy the famous Mukhanov-Sasaki equation given by [58, 59]

$$v_k'' + \left(k^2 - \frac{z''}{z} \right) v_k = 0, \quad (\text{A.4})$$

where the potential term is given by the following exact expression [67]

$$\frac{z''}{z} = a^2 H^2 \left(2 - \epsilon_1 + \frac{3}{2} \epsilon_2 + \frac{1}{4} \epsilon_2^2 - \frac{1}{2} \epsilon_1 \epsilon_2 + \frac{1}{2} \epsilon_2 \epsilon_3 \right), \quad (\text{A.5})$$

with $\epsilon_1 = \epsilon_H$ and

$$\epsilon_{n+1} = -\frac{d \ln \epsilon_n}{dN_e} . \quad (\text{A.6})$$

Given a mode k , at sufficiently early times when it is sub-Hubble i.e $k \gg aH$, we can assume v to be in the Bunch-Davis vacuum [108] satisfying

$$v_k \rightarrow \frac{1}{\sqrt{2k}} e^{-ik\tau} . \quad (\text{A.7})$$

During inflation as the comoving Hubble radius falls, this mode starts becoming super-Hubble i.e $k \ll aH$ and equation (A.4) dictates that $|v_k|$ approaches a constant value. We numerically compute this asymptotically constant super-Hubble values of the real and imaginary parts of v_k by solving the Mukhanov-Sasaki equation and estimate the dimensionless primordial power-spectrum of \mathcal{R} using the following relation [49, 107]

$$P_{\mathcal{R}} = \frac{k^3}{2\pi^2} \frac{|v_k|^2}{z^2} \Big|_{k \ll aH} . \quad (\text{A.8})$$

During the slow-roll inflation, the factor $\frac{z''}{z} = \frac{\nu^2 - 0.25}{\tau^2}$ with $\nu \approx 1.5 + \epsilon_H + \frac{\epsilon_H}{2H\epsilon_H}$. The solution to Mukhanov-Sasaki equation with suitable Bunch-Davis vacuum conditions picks up the Hankel function of first kind $H_\nu^{(1)}$ and the subsequent computation of the power spectrum of \mathcal{R} leads to the famous slow-roll approximation formula (2.8). When the slow-roll condition (2.7) is violated, but by not more than $\mathcal{O}(1)$, one could still come up with higher order analytical results for $P_{\mathcal{R}}$ which are more accurate compared to (2.8) as described in [48]. However to be absolutely accurate, we have relied upon the numerical solution of (A.4) for computation of $P_{\mathcal{R}}$ for calculating PBH mass function.

Note that numerically, one could also directly try to solve for the fourier modes of the comoving curvature perturbation \mathcal{R} which satisfy the equation

$$\mathcal{R}_k'' + 2 \left(\frac{z'}{z} \right) \mathcal{R}_k' + k^2 \mathcal{R}_k = 0 \quad (\text{A.9})$$

and implement the corresponding Bunch-Davis initial conditions for \mathcal{R}_k .

B Primordial black hole formation and abundance

Mass of PBHs formed at a certain epoch in the radiation dominated era, due to Hubble re-entry of a large fluctuation mode k_{PBH} , is given by the Hubble mass at that epoch (upto an efficiency factor $\gamma \simeq 0.2$).

$$M_{\text{PBH}} = \gamma M_H = \gamma \frac{4\pi m_p^2}{H} \quad (\text{B.1})$$

Where the Hubble scale during radiation dominated epoch ($\rho_{\text{tot}} \simeq \rho_r$) is given by

$$H^2 = \frac{\rho_{\text{tot}}}{3m_p^2} = \frac{\rho_r}{3m_p^2} = \Omega_{0r} H_0^2 \frac{\rho_r}{\rho_{0r}} ,$$

with

$$\frac{\rho_r}{\rho_{0r}} = \frac{g_*}{g_{0*}} \left(\frac{T}{T_0} \right)^4 ,$$

where g_* is the effective number of relativistic degrees of freedom of the energy density and its present value given by $g_{0*} = 3.38$, assuming $N_{\text{eff}} = 3.046$. From entropy conservation, we have

$$\left(\frac{T}{T_0}\right)^4 = \left(\frac{g_*^s}{g_{0*}^s}\right)^{-4/3} (1+z)^4 ,$$

where g_*^s is the effective number of relativistic degrees of freedom of entropy density and its present value given by $g_{0*}^s = 3.94$. Assuming $g_* = g_*^s$ deep within the radiation dominated epoch at very early times, we get

$$H^2 = \Omega_{0r} H_0^2 (1+z)^4 \left(\frac{g_*}{g_{0*}}\right)^{-1/3} \left(\frac{g_{0*}^s}{g_{0*}}\right)^{4/3} . \quad (\text{B.2})$$

Expression (B.2) can be further simplified in the form

$$H^2 = \Omega_{0r} h^2 \times \left(\frac{100 \text{ km}}{\text{s Mpc}}\right)^2 \left(\frac{g_*}{g_{0*}}\right)^{-1/3} \left(\frac{g_{0*}^s}{g_{0*}}\right)^{4/3} (1+z)^4 . \quad (\text{B.3})$$

Inserting (B.2) in (B.1), converting from natural units $c, \hbar = 1$ to S.I units and using $M_\odot = 1.99 \times 10^{30} \text{ kg}$, $\Omega_{0r} h^2 = 4.18 \times 10^{-5}$ we get

$$\frac{M_{\text{PBH}}}{M_\odot} = 4.83 \times 0.2 \times 10^{24} \left(\frac{\gamma}{0.2}\right) \left(\frac{g_*}{g_{0*}}\right)^{1/6} \left(\frac{g_{0*}^s}{g_{0*}}\right)^{-2/3} (1+z)^{-2} , \quad (\text{B.4})$$

which, after substituting the value of g_{0*} and g_{0*}^s becomes

$$\frac{M_{\text{PBH}}}{M_\odot} = 1.55 \times 10^{24} \left(\frac{\gamma}{0.2}\right) \left(\frac{g_*}{106.75}\right)^{1/6} (1+z)^{-2} . \quad (\text{B.5})$$

In order to establish the relation between M_{PBH} and k_{PBH} given in expression (3.14), we proceed as follows.

$$\Delta N = N_* - N_e^{\text{PBH}} = \ln \frac{a_{\text{exit}}}{a_*} = \ln \frac{a_{\text{exit}} H_*}{k_*}$$

Assuming the Hubble scale during inflation to be roughly constant i.e $a_{\text{exit}} H_* \simeq a_{\text{exit}} H_{\text{exit}}$, we get

$$\Delta N = N_* - N_e^{\text{PBH}} = \ln \frac{a_{\text{exit}} H_{\text{exit}}}{k_*} = \ln \frac{(aH)_{\text{PBH}}}{k_*} ,$$

which can be written as

$$\Delta N = N_* - N_e^{\text{PBH}} = \ln \left[\frac{H_{\text{PBH}}}{(1+z)k_*} \right] . \quad (\text{B.6})$$

Substituting the expression for H_{PBH} from (B.3) and converting all redshift dependence to mass dependence from (B.5), we get the relation between $N_* - N_e^{\text{PBH}}$ and M_{PBH} as given in (3.15)

$$N_* - N_e^{\text{PBH}} = 17.33 + \frac{1}{2} \ln \frac{\gamma}{0.2} - \frac{1}{12} \ln \frac{g_*}{106.75} - \frac{1}{2} \ln \frac{M_{\text{PBH}}}{M_\odot} . \quad (\text{B.7})$$

Using the fact that $k_{\text{PBH}} = (aH)_{\text{PBH}} = (aH)_{\text{exit}}$, $k_* = (aH)_*$ and assuming $H_* \simeq H_{\text{exit}}$, we have

$$k_{\text{PBH}} = k_* e^{(N_* - N_e^{\text{PBH}})}, \quad (\text{B.8})$$

which upon substitution into equation (B.7) yields

$$\frac{M_{\text{PBH}}}{M_\odot} = 1.13 \times 10^{15} \left(\frac{\gamma}{0.2} \right) \left(\frac{g_*}{106.75} \right)^{-1/6} \left(\frac{k_{\text{PBH}}}{k_*} \right)^{-2}, \quad (\text{B.9})$$

which can also be written as [49]

$$M_{\text{PBH}} = 1.36 \times 10^{18} g \left(\frac{\gamma}{0.2} \right) \left(\frac{g_*}{106.75} \right)^{-1/6} \left(\frac{k_{\text{PBH}}}{7 \times 10^{13} \text{Mpc}^{-1}} \right)^{-2}. \quad (\text{B.10})$$

The mass fraction of PBHs at formation is defined as

$$\beta(M_{\text{PBH}}) = \frac{\rho_{\text{PBH}}}{\rho_{\text{tot}}} \Big|_{\text{formation}}. \quad (\text{B.11})$$

Assuming that PBHs redshift as matter after formation we have

$$\beta(M_{\text{PBH}}) = \frac{\rho_{\text{PBH}}}{3m_p^2 H_0^2} \left(\frac{H_0}{H} \right)^2 = \frac{\rho_{0\text{PBH}}}{3m_p^2 H_0^2} (1+z)^3 \left(\frac{H_0}{H} \right)^2 = \frac{\rho_{0\text{DM}}}{3m_p^2 H_0^2} \frac{\rho_{0\text{PBH}}}{\rho_{0\text{DM}}} (1+z)^3 \left(\frac{H_0}{H} \right)^2.$$

Hence we have

$$\beta(M_{\text{PBH}}) = \Omega_{0\text{DM}} f_{\text{PBH}}(M_{\text{PBH}}) \left(\frac{H_0}{H} \right)^2 (1+z)^3, \quad (\text{B.12})$$

where $f_{\text{PBH}}(M_{\text{PBH}})$ is the mass function of fractional abundance of PBHs defined by

$$f_{\text{PBH}} = \frac{\Omega_{0\text{PBH}}}{\Omega_{0\text{DM}}} \quad (\text{B.13})$$

Substituting the expressions for H and z in terms of $\frac{M_{\text{PBH}}}{M_\odot}$ from equations (B.3) and (B.5), we get

$$\beta(M_{\text{PBH}}) = 5.95 \times 10^{-9} \left(\frac{\gamma}{0.2} \right)^{-1/2} \left(\frac{M_{\text{PBH}}}{M_\odot} \right)^{1/2} \left(\frac{g_*}{106.75} \right)^{1/4} f_{\text{PBH}}(M_{\text{PBH}}). \quad (\text{B.14})$$

Since $\beta(M_{\text{PBH}})$ can be computed from the primordial power spectrum $P_{\mathcal{R}}$ using Press-Schechter (or peak theory) formalism, we invert this expression to get the mass function of fractional PBH abundance as

$$f_{\text{PBH}}(M_{\text{PBH}}) = 1.68 \times 10^8 \left(\frac{\gamma}{0.2} \right)^{1/2} \left(\frac{g_*}{106.75} \right)^{-1/4} \left(\frac{M_{\text{PBH}}}{M_\odot} \right)^{-1/2} \beta(M_{\text{PBH}}) \quad (\text{B.15})$$

References

- [1] Ya.B. Zel'dovich and I.D. Novikov, Sov. Astron. **10**, 602 (1967).
- [2] S.W. Hawking, Nature (London) **248**, 30 (1974).
- [3] B. J. Carr and S. W. Hawking, Mon. Not. Roy. Astron. Soc. **168**, 399 (1974).
- [4] B.J. Carr, Astroph. J. **201**, 1 (1975).

- [5] D. N. Page and S. W. Hawking, *Astrophys. J.* **206**, 1 (1976).
- [6] Ya. B. Zeldovich and A. A. Starobinsky, *Pisma Zh. Eksp. Teor. Fiz.* **24**, 616 (1976).
- [7] P. D. Naselsky, *Pisma Astron. Zh.* **4**, 387 (1978); *Sov. Astron. Lett.* **4**, 209 (1978).
- [8] I. D. Novikov, A. G. Polnarev, A. A. Starobinsky, and Ya. B. Zeldovich, *Astron. Astrophys.* **80**, 104 (1979).
- [9] S. Miyama and K. Sato, *Prog. Theor. Phys.* **59**, 1012 (1978).
- [10] D. Lindley, *Mon. Not. R. Astron. Soc.* **193**, 593 (1980).
- [11] A. F. Heckler, *Phys. Rev. Lett.* **78**, 3430 (1997).
- [12] B.J. Carr and M.J. Rees, *Mon. Not. Roy. Ast. Soc.* **206**, 801 (1984).
- [13] R. Bean and J. Magueijo, *Phys. Rev. D* **66**, 063505 (2002).
- [14] N. Afshordi, P. McDonald and D.N. Spergel, *Astroph. J. Lett.* **594**, L71 (2003).
- [15] K.M. Belotsky and A.A. Kirillov, *JCAP* **1501**(01), 041 (2015).
- [16] G.F. Chapline, *Nature (London)* **253**, 251 (1975).
- [17] P. Meszaros, *Astron. Astrophys.* **38**, 5 (1975)
- [18] D. Blais, C. Kiefer and D. Polarski, *Phys. Lett. B* **535**, 11 (2002).
- [19] S. Bird, I. Cholis, J. B. Muoz, Y. Ali-Hamoud, M. Kamionkowski, E. D. Kovetz, A. Raccanelli, and A. G. Riess, *Phys. Rev. Lett.* **116**, 201301 (2016), [arXiv:1603.00464 [astro-ph.CO]].
- [20] S. Clesse and J. Garca-Bellido, *Phys. Dark Univ.* **15**, 142 (2017), [arXiv:1603.05234 [astro-ph.CO]].
- [21] M. Sasaki, T. Suyama, T. Tanaka, and S. Yokoyama, *Phys. Rev. Lett.* **117**, 061101 (2016), [arXiv:1603.08338 [astro-ph.CO]].
- [22] M. Kawasaki, A. Kusenko, Y. Tada, and T. T. Yanagida, *Phys. Rev. D* **94**, 083523 (2016), [arXiv:1606.07631 [astro-ph.CO]].
- [23] B. Carr, F. Kuhnel, and M. Sandstad, *Phys. Rev. D* **94**, 083504 (2016), [arXiv:1607.06077 [astro-ph.CO]].
- [24] K. Inomata, M. Kawasaki, K. Mukaida, Y. Tada, and T. T. Yanagida, *Phys. Rev. D* **95**, 123510 (2017), [arXiv:1611.06130 [astro-ph.CO]].
- [25] K. Inomata, M. Kawasaki, K. Mukaida, Y. Tada and T. T. Yanagida, *Phys. Rev. D* **96**, no. 4, 043504 (2017) [arXiv:1701.02544 [astro-ph.CO]].
- [26] T. Nakama, J. Silk, and M. Kamionkowski, *Phys. Rev. D* **95**, 043511 (2017), [arXiv:1612.06264 [astro-ph.CO]].
- [27] F. Khnel and K. Freese, *Phys. Rev. D* **95**, 083508 (2017), [arXiv:1701.07223 [astro-ph.CO]].
- [28] T. Chiba and S. Yokoyama, *PTEP* **8**, 083 (2017), [arXiv:1704.06573 [gr-qc]].
- [29] B. Carr, M. Raidal, T. Tenkanen, V. Vaskonen, and H. Veerme, *Phys. Rev. D* **96**, 023514 (2017), [arXiv:1705.05567 [astro-ph.CO]].
- [30] V. Domcke, F. Muia, M. Pieroni and L.T. Witkowski, [arXiv:1704.03464].
- [31] Y. Tada and S. Yokoyama, [arXiv:1904.10298].
- [32] B. J. Carr, K. Kohri, Y. Sendouda and J. Yokoyama, *Phys. Rev. D* **81**, 104019 (2010) [arXiv:0912.5297 [astro-ph.CO]].
- [33] S. Passaglia, W. Hu and H. Motohashi, *Phys. Rev. D* **99**, 043536 (2019).
- [34] B.P. Abbott et al, (LIGO Scientific and Virgo Collaborations) *Phys. Rev. D* **96**, 023514 (2016).

- [35] S. Wang, Y. F. Wang, Q. G. Huang and T. G. F. Li, Phys. Rev. Lett. **120**, no. 19, 191102 (2018) [arXiv:1610.08725 [astro-ph.CO]].
- [36] S. Wang, T. Terada and K. Kohri, Phys. Rev. D **99**, no. 10, 103531 (2019) [arXiv:1903.05924 [astro-ph.CO]].
- [37] M. Yu. Khlopov, Research in Astron. Astrophys. **2010**, 495 (2010).
- [38] M. Sasaki, T. Suyama, T. Tanaka and S. Yokoyama, Class. Quantum Grav. **35**, 063001 (2018).
- [39] D.S. Salopek, J.R. Bond and J.M. Bardeen, Phys. Rev. D **40**, 1753 (1989).
- [40] V.F. Mukhanov and M.I. Zelnikov, Phys. Lett. B **263**, 169 (1991).
- [41] A.A. Starobinsky, JETP Lett. **55**, 489 (1992).
- [42] J. Garcia-Bellido, A. Linde and D. Wands, Phys. Rev. D **54**, 6040 (1996).
- [43] L. Randall, N. Sikjadic and A. Guth, Phys. Lett. B **472**, 377 (1996).
- [44] P. Ivanov, P. Nasselsky and I.D. Novikov, Phys. Rev. D **50**, 7173 (1994).
- [45] P. Ivanov, Phys. Rev. D **57**, 7145 (1998).
- [46] C. Germani and T. Prokopec, Physics of the Dark Universe, **18**, 6 (2017).
- [47] J. Garcia-Bellido and E.R. Morales, Physics of the Dark Universe, **18**, 47 (2017).
- [48] H. Motohashi and W. Hu, Phys. Rev. D **96**, 063503 (2017).
- [49] G. Ballesteros and M. Taoso, Phys. Rev. D **97**, 023501 (2018).
- [50] N. Bhaumik and R. K. Jain, [arXiv:1907.04125 [astro-ph.CO]].
- [51] M. Cicoli, V. A. Diaz and F. G. Pedro, JCAP **1806**, 034 (2018) [arXiv:1803.02837 [hep-th]].
- [52] S. Kachru, R. Kallosh, A. Linde and S. P. Trivedi, Phys. Rev. D **68**, 046005 (2003), [hep-th/0301240]
- [53] S. Kachru, R. Kallosh, A. D. Linde, J. M. Maldacena, L. P. McAllister and S. P. Trivedi, JCAP **0310**, 013 (2003) [hep-th/0308055].
- [54] R. Kallosh and A. Linde, JCAP07 (2013) 002 [arXiv:1306.5220].
- [55] R. Kallosh, A. Linde and D. Roest, JHEP11, 198 (2013) [arXiv:1311.0472].
- [56] S. S. Mishra, V. Sahni and A. V. Toporensky, Phys. Rev. D **98**, no. 8, 083538 (2018) [arXiv:1801.04948 [gr-qc]].
- [57] D. Baumann, [arXiv:0907.5424 [hep-th]].
- [58] M. Sasaki, Prog. Theor. Phys. **76**, 1036 (1986).
- [59] V. F. Mukhanov, Sov. Phys. JETP **67**, 1297 (1988) [Zh. Eksp. Teor. Fiz. **94N7**, 1 (1988)]
- [60] Y. Akrami *et al.* [Planck Collaboration], [arXiv:1807.06211 [astro-ph.CO]].
- [61] P. A. R. Ade *et al.* [BICEP2 and Keck Array Collaborations], Phys. Rev. Lett. **121**, 221301 (2018) [arXiv:1810.05216 [astro-ph.CO]].
- [62] R. Kallosh, A. Linde and Y. Yamada, JHEP **1901**, 008 (2019) [arXiv:1811.01023 [hep-th]].
- [63] R. Kallosh and A. Linde, JCAP **1909**, no. 09, 030 (2019) [arXiv:1906.02156 [hep-th]].
- [64] R. Kallosh and A. Linde, arXiv:1909.04687 [hep-th].
- [65] R. Kallosh and A. Linde, arXiv:1906.04729 [astro-ph.CO].
- [66] V. Atal, J. Garriga and A. Marcos-Caballero, JCAP **1909**, no. 09, 073 (2019) [arXiv:1905.13202 [astro-ph.CO]].

- [67] H. Motohashi, A. A. Starobinsky and J. Yokoyama, JCAP **1509**, 018 (2015) [arXiv:1411.5021 [astro-ph.CO]].
- [68] H. Motohashi, S. Mukohyama and M. Oliosi, [arXiv:1910.13235 [gr-qc]].
- [69] A. A. Starobinsky, Phys. Lett. **91B**, 99 (1980).
- [70] I. Dalianis, A. Kehagias and G. Tringas, JCAP **1901**, 037 (2019) [arXiv:1805.09483 [astro-ph.CO]].
- [71] R. Mahbub, [arXiv:1910.10602 [astro-ph.CO]].
- [72] C. Germani and I. Musco, Phys. Rev. Lett. **122**, no. 14, 141302 (2019) [arXiv:1805.04087 [astro-ph.CO]].
- [73] B. Carr, M. Raidal, T. Tenkanen, V. Vaskonen and H. Veerme, Phys. Rev. D **96**, no. 2, 023514 (2017) [arXiv:1705.05567 [astro-ph.CO]].
- [74] S. Young, C. T. Byrnes, and M. Sasaki, JCAP **1407** (2014) 045, [arXiv:14.05.7023]
- [75] I. Musco, [arXiv:1809.02127].
- [76] C.-M. Yoo, T. Harada, J. Garriga, and K. Kohri, [arXiv:1805.03946].
- [77] W. H. Press and P. Schechter, Astrophys. J. **187**, 425 (1974).
- [78] T Harada, C.-M. Yoo, and K. Kohri, Phys. Rev. D **88**, 084051 (2013)
- [79] A. M. Green, A. R. Liddle, K. A. Malik and M. Sasaki, Phys. Rev. D **70** (2004) 041502 [astro-ph/0403181].
- [80] M. Shibata and M. Sasaki, Phys. Rev. D **60** (1999) 084002 [gr-qc/9905064].
- [81] I. Musco, J. C. Miller and A. G. Polnarev, Class. Quant. Grav. **26**, 235001 (2009) [arXiv:0811.1452 [gr-qc]].
- [82] A. G. Polnarev and I. Musco, Class. Quant. Grav. **24**, 1405 (2007) [gr-qc/0605122].
- [83] A. Escrivá, C. Germani and R. K. Sheth, arXiv:1907.13311 [gr-qc].
- [84] A. Escrivá, [arXiv:1907.13065 [gr-qc]].
- [85] S. Young, arXiv:1905.01230 [astro-ph.CO].
- [86] K. Ando, K. Inomata and M. Kawasaki, Phys. Rev. D **97**, no. 10, 103528 (2018) doi:10.1103/PhysRevD.97.103528 [arXiv:1802.06393 [astro-ph.CO]].
- [87] H. Niikura *et al.*, Nat. Astron. **3**, no. 6, 524 (2019) [arXiv:1701.02151 [astro-ph.CO]].
- [88] N. Bartolo, V. De Luca, G. Franciolini, A. Lewis, M. Peloso and A. Riotto, Phys. Rev. Lett. **122**, no. 21, 211301 (2019) [arXiv:1810.12218 [astro-ph.CO]].
- [89] C. T. Byrnes, P. S. Cole and S. P. Patil, JCAP **1906**, 028 (2019) [arXiv:1811.11158 [astro-ph.CO]].
- [90] O. Ozsoy and G. Tasinato, [arXiv:1912.01061 [astro-ph.CO]].
- [91] S. Clesse and J. Garca-Bellido, Phys. Rev. D **92**, no. 2, 023524 (2015) [arXiv:1501.07565 [astro-ph.CO]].
- [92] D. Baumann, P. J. Steinhardt, K. Takahashi and K. Ichiki, Phys. Rev. D **76**, 084019 (2007) [hep-th/0703290].
- [93] J. Garcia-Bellido, M. Peloso and C. Unal, JCAP **1709**, 013 (2017) [arXiv:1707.02441 [astro-ph.CO]].
- [94] S. Clesse, J. Garca-Bellido and S. Orani, arXiv:1812.11011 [astro-ph.CO].
- [95] M. Raidal, V. Vaskonen and H. Veerme, JCAP **1709**, 037 (2017) [arXiv:1707.01480 [astro-ph.CO]].

- [96] R. g. Cai, S. Pi and M. Sasaki, Phys. Rev. Lett. **122**, no. 20, 201101 (2019) [arXiv:1810.11000 [astro-ph.CO]].
- [97] C. Pattison, V. Vennin, H. Assadullahi and D. Wands, JCAP **1710**, 046 (2017) [arXiv:1707.00537 [hep-th]].
- [98] J. M. Ezquiaga and J. Garca-Bellido, JCAP **1808**, 018 (2018) [arXiv:1805.06731 [astro-ph.CO]].
- [99] M. Biagetti, G. Franciolini, A. Kehagias and A. Riotto, JCAP **1807**, 032 (2018) [arXiv:1804.07124 [astro-ph.CO]].
- [100] S. Young and C. T. Byrnes, JCAP **1308**, 052 (2013) [arXiv:1307.4995 [astro-ph.CO]].
- [101] S. Young, D. Regan and C. T. Byrnes, JCAP **1602**, 029 (2016) [arXiv:1512.07224 [astro-ph.CO]].
- [102] G. Franciolini, A. Kehagias, S. Matarrese and A. Riotto, JCAP **1803**, 016 (2018) [arXiv:1801.09415 [astro-ph.CO]].
- [103] C. T. Byrnes, E. J. Copeland and A. M. Green, Phys. Rev. D **86**, 043512 (2012) [arXiv:1206.4188 [astro-ph.CO]].
- [104] V. De Luca, G. Franciolini, A. Kehagias, M. Peloso, A. Riotto and C. nal, JCAP **1907**, 048 (2019) [arXiv:1904.00970 [astro-ph.CO]].
- [105] V. Atal and C. Germani, Phys. Dark Univ. **24**, 100275 (2019) [arXiv:1811.07857 [astro-ph.CO]].
- [106] V. Atal, J. Cid, A. Escriv and J. Garriga, [arXiv:1908.11357 [astro-ph.CO]].
- [107] D. Baumann, PoS TASI **2017**, 009 (2018) [arXiv:1807.03098 [hep-th]].
- [108] T. S. Bunch and P. C. W. Davies, Proc. Roy. Soc. Lond. A **360**, 117 (1978).